

Michael Töfferl, BSc

Inline Monitoring of Thermal Resistances for LED Packages

Master's Thesis

to achieve the university degree of

DIPLOM-INGENIEUR

Master's degree programme:

TECHNICAL PHYSICS

submitted to

Graz University of Technology

SUPERVISOR

Ass.Prof. Priv.-Doz. Dipl.-Phys. Dr.rer.nat. Karin Zojer

Institute of Solid State Physics

in cooperation with Materials Center Leoben Forschung GmbH (MCL)

Graz, August 2022

AFFIDAVIT

I declare that I have authored this thesis independently, that I have not used other than the declared sources/resources, and that I have explicitly indicated all material which has been quoted either literally or by content from the sources used. The text document uploaded to TUGRAZonline is identical to the present master's thesis.

(Date)

(Signature)

Acknowledgement

This was a long lasting journey for myself and I am thankful that people around me helped me in my most desperate times. Writing a diploma thesis for the first time is and was a great pleasure and I am sure there are always ups and downs. For me this project now has finally come to an end where I personally can thank all who kept me pushing.

First I would like to thank my family who were always there for me and tried to support me in every way. I also want to mention my friends and study colleagues who were nearly in the same game. It is a lot easier to work on problems together, try to get different approaches, or simply letting you know that you are wrong. This always applied in my years as a physics student.

And last I want to thank my supervisors who supported me with great knowledge in this field. Karin Zojer as my supervisor at the TU Graz, showing me how to find new ways to tackle a problem. And Julien Magnien who supported me all this time and was there whenever I needed a talk.

The author gratefully acknowledges the financial support under the scope of the COMET program within the K2 Center “Integrated Computational Material, Process and Product Engineering (IC-MPPE)” (Project No 859480). This program is supported by the Austrian Federal Ministries for Climate Action, Environment, Energy, Mobility, Innovation and Technology (BMK) and for Digital and Economic Affairs (BMDW), represented by the Austrian research funding association (FFG), and the federal states of Styria, Upper Austria and Tyrol.

Abstract

Safety and prediction of failures for technical components are particularly important. Semiconductor devices, which are used more and more often in everyday life, play a special role in security. Depending on the use case, a failure in semiconductor elements can be crucial, especially in the area of lighting. LEDs (Light Emitting Diodes) are present in a wide range of applications like displays or lighting, where sometimes safety is an important issue. Just to mention the automotive industry, where LEDs are used for control panel displays as well as headlights illuminating the streets. The failure of headlights in the night can pose a particularly serious safety risk. A reliable early warning system would reduce the risk of sudden failure while improving the safety. Error detection is one of the tasks of LED monitoring. With the support of LED monitoring systems, the health state of the lighting and displays can be checked. If deviations from the normal operation mode are observed, the system can alert the user in order to prevent serious failures from happening.

In this thesis a monitoring system was developed, which is able to monitor the operation state of the LED during its lifetime. The monitoring is implemented using the structure function, which relates to the physical layers in the system as thermal resistances. The starting point for calculating the structure function is the transient measurement of the voltage, which can be done with the compact measurement unit. The measuring unit records voltage transients of the LED as a step response to a change in power and transmits the data to the evaluation program. The main task of the evaluation program is the quick and easy calculation of the structure function in order to enable monitoring “inline” direct after the measurement. The monitoring system shows the thermal resistances for specially selected layers in the system, which can be responsible for errors. Depending on the type of error in the LED, changes occur for the respective thermal resistances, which are immediately evaluated and visualized with each new measurement. Errors and error causes for the LED can be clearly determined via the characteristic profiles for the thermal resistance. This enables early detection of errors for the LED.

Kurzfassung

Sicherheit und Voraussage von Fehlern bei technische Bauteilen sind besonders wichtig. Halbleiterbauelemente, die immer mehr im Alltag eingesetzt werden, spielen eine besondere Rolle für Sicherheit. Je nach Anwendung kann ein Ausfall von Halbleiterbauelementen besonders fatal sein. Im Bereich Beleuchtung tritt dieser Fall ein. LEDs (Light Emitting Diode) treten in einem extrem breiten Spektrum von Einsatzmöglichkeiten auf, bei welchen Sicherheit eine Rolle spielt. Sei es für Anwendungen im Verkehr, zum Ausleuchten von Gehwegen oder für Automobile. Es werden immer mehr LED Scheinwerfer in Autos verbaut. Der Ausfall von Scheinwerfer in der Nacht kann ein besonders großes Sicherheitsrisiko darstellen. Ein verlässliches Frühwarnsystem wäre praktisch für die Detektierung/Warnung von Ausfällen. Fehlererkennung ist eine der Aufgaben von LED Monitoring. Mit Hilfe von LED Monitoring kann der Zustand der LED und des ganzen Systems überwacht werden. Bei Änderungen oder Abweichungen des Normalbetriebs kann das Monitoring System einschreiten.

In der Arbeit wurde ein Monitoring System entwickelt, welches den Zustand der LED während der Lebenszeit überwacht. Das Monitoring wird mit Hilfe der Strukturfunktion umgesetzt, welche die physischen Schichten im System als thermische Widerstände angibt. Ausgangspunkt für die Berechnung der Strukturfunktion sind die Transientenmessungen, welche über die eigens entwickelte Messeinheit stattfinden. Die Messeinheit zeichnet Spannungstransienten der LED als Sprungantwort einer Leistungsänderung auf und übermittelt die Daten an das Auswertungs-Programm. Die Hauptaufgabe des Auswertungs-Programms liegt in der schnellen und einfachen Berechnung der Strukturfunktion, um das Monitoring "inline" mit der Messung zu ermöglichen. Das Monitoring zeigt die thermischen Widerstände für speziell ausgewählte Schichten im System an, welche für Fehler verantwortlich sein können. Je nach Fehlerart der LED entstehen Änderungen für die jeweiligen thermischen Widerstände, welche mit jeder neuen Messung sofort ausgewertet und visualisiert werden. Über die charakteristischen Profile für den thermischen Widerstand können Fehler und Fehlerursachen für die LED eindeutig ermittelt werden. Damit wird eine frühzeitige Erkennung von Fehlern für die LED ermöglicht.

Contents

Abstract	3
Kurzfassung	4
Contents	5
1 Motivation	7
2 Fundamental aspects	8
2.1 What does “Inline Monitoring” mean?	8
2.2 Lifetime estimations for LEDs	8
2.3 Network analysis via temperature transients	9
3 Design under Test (DuT)	12
3.1 Diode characteristics	13
4 TSEP measurement unit	18
4.1 Measurement device parameters	18
4.2 Working principle	19
4.3 Trouble shooting	20
4.3.1 Time shift	20
4.3.2 Data Points	22
4.3.3 Incorrect measurements	22
4.3.4 Time for measurements	22
5 Processing with structure functions	24
5.1 Structure function as a tool	24
5.2 Computation steps of the structure function	24
5.2.1 Preparation	24
5.2.2 Calculation	26
5.3 Benchmarking	28
5.3.1 Validation with different systems	29
5.3.2 Time and CPU consumption	35
5.3.3 Error estimation of parameters	37
6 RC-network reduction	39
6.1 Temperature transient reconstruction from RC-networks	39

6.1.1	Network transformation from Cauer network to Foster network	39
6.1.2	Temperature response validation with cost function	41
6.2	Network reduction with structure function	41
7	Inline monitoring	45
7.1	Monitoring process flow	45
7.2	Long term test	48
7.2.1	Experimental setup	48
7.2.2	Results from measurements	50
8	Summary	56
	List of Figures	62
	List of Tables	66
	List of Listings	67

1 Motivation

Semiconductor devices are present in our everyday life more than ever. The smartphone industry, sensors in measurement devices, or lighting industry just to mention a few; it is hard to imagine a world without these application areas. All these devices are still developed further to push the limits in terms of their size and efficiency. One big area are LEDs (light emitting diode), which removed the old classical light bulb in the last years. LEDs are very efficient in energy consumption and lifetime compared to other light sources. There are two main field of use, namely for displays and for lighting. Depending on the use case, LEDs must meet certain criteria with respect to brightness or reliability. In traffic transport e.g., traffic lights must not break down or headlights of a car must work properly in the dark. In these application areas it is crucial to have reliable devices. Even more it would be a great safety feature to predict the moment in time, when a device fails, in order to replace it before further damage can happen.

Redundancy is in most cases a good approach to prevent total failure. Overhead projectors for example, were equipped with two light bulbs. If one fails, the other bulb can be used to continue. Nevertheless, this security strategy is not optimal in case of cost and space, sometimes it simply is not possible to maintain two separate devices/systems. Another approach to check the “health state” of the device would be more desirable. In a battery, for example, the state of charge can be checked via the open-circuit voltage, whether you have an old battery or a new one. For an LED it would be useful to know the age or its functionality, to give information about its failure probability. Depending on that a device can be replaced or adjusted to obtain a higher lifetime.

The age of an LED is noticeable described by two main phenomena, a rise in operation temperature and a change in light output [1, 2, 3]. These two parameters allow lifetime estimation. A LED can be said broken per definition when its brightness level is below a certain value. Depending on its brightness profile over time, predictions can be made about age and remaining lifetime. Usually this is not a practicable method in real applications because brightness measurements typically cannot be done in situ. Temperature measurements are feasible. One possible measurement route places a temperature sensor at some point and compares the values. In a second, more basic approach, the applied voltage can be used as a temperature reference, since semiconductor devices hold a voltage-temperature relation [4, 5, 6, 7]. Once a reference measurement is done, the temperature and even a thermal resistance can be obtained, which both relate to the “health state” of the device. The higher the thermal resistance, the higher the less efficient heat is dissipated and temperature of the device, which is an indicator for failure mechanisms [8]. If heat dissipation is not guaranteed, wear and tear or damage to the component will occur. Most failure types such as fatigue failures can be noticed as changes in the thermal resistance [1]. Therefore, the thermal resistance of an LED is suitable as analysis tool to estimate remaining lifetime and to also detect failures in the device.

To extend this idea even further, the thermal resistance can be split up into resistances of single components in the LED-system [9, 10, 11]. Every resistance then can represent a physical layer (e.g., chip, thermal interface, etc.) which changes due to failures. If these changes can somehow be “monitored live”, not only failures could be detected but might even be prevented. Combining this method with safety devices like headlights, highly improves security and safety. Maintenance based on the analysis of thermal resistances, i.e. on detailed failure reports could lead to a lower failure rate.

2 Fundamental aspects

2.1 What does “Inline Monitoring” mean?

The term “inline monitoring” in this context refers to the monitoring of an LED in use during its lifetime. Because LEDs are used in various fields of application, it is useful to monitor its age, or in other words, its “health status”. This means one is able to estimate its remaining lifetime or in the best case, predict a failure. Monitoring the LED can be achieved by measuring quantities, which are described later in this thesis. There are certain instruments involved, which perform the measurement to gain the information which is needed. The word “inline” describes the analysis process. The goal of inline monitoring is to use a compact setup, which is capable of measuring and computing the results fast and on-the-fly. The results should not depend on further instruments weather to confirm the “health state” of the LED. All combined, this tool can help to determine the failure mechanisms that occur during use of the LED. Depending on the analysis, “inline monitoring” detects not only changes, but also permits detailed investigations on failures in real time.

2.2 Lifetime estimations for LEDs

There are two categories for LED failures: Catastrophic and parametric failures [12, 13]. Catastrophic failures are sudden and permanent disorders in the device. They can happen at any time, but typically occur at a rather early operation period of an LED. They can be difficult to observe, since no hint in structural change signals a failure in advance. Examples can be voltage drops/peaks or user errors. Parametric failures are systematic failures, which are observable in long term operation. Often, they can be referred to wear and tear. They are perfect for inline monitoring, where changes over time can be recorded and analysed [14, 15]. The time for total break down due to parametric failures is most likely at the end of the LED’s lifetime, due to long degeneration times. In fig. 1 the failure rate (dotted line) of two different LED products can be seen. The characteristic shape is a “bathtub”, i.e., failure peaks are present at the beginning and at the end of lifetime. These peaks are related to the catastrophic and parametric failures, respectively.

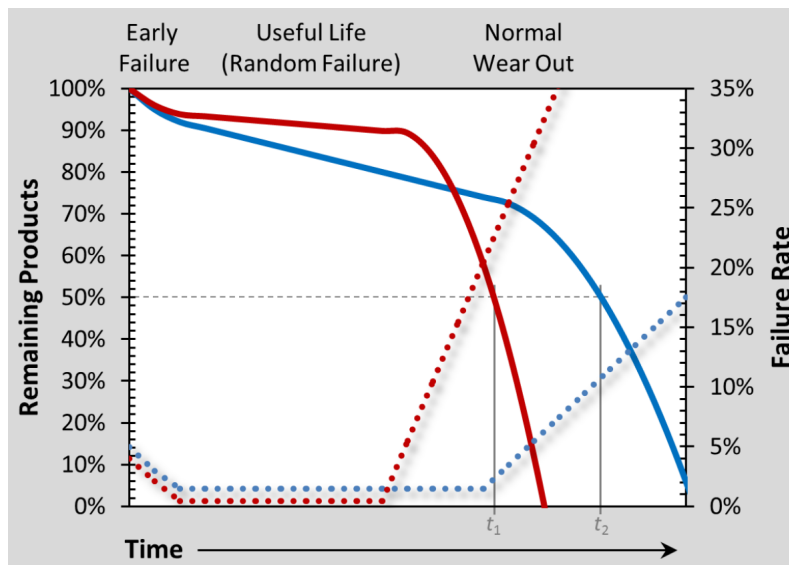


Figure 1: Failure rate (dotted lines) and percentage remaining products (solid lines) for two hypothetical products with different life time estimations at 50% failures. [16]

In the case of parametric failures, there are two types of parameter changes, that are most commonly observed: Temperature increase and changes in light output. Both can be used to model and estimate lifetime. Considering the light output, the lifetime of the LED is defined such as, when the light output is 70 percent of the initial value. The value is described as L70 and uses the LM-80 [17, 18] test data TM-21 [19] extrapolation to calculate the life expectancy of an LED device. The LED is operated under standard conditions and the light output is measured for at least 6000 hours. The value of the lumen maintenance can be extrapolated up to 70 percent to estimate its lifetime. L70 is mostly used in the lighting industry while L50 (50 percent light degradation) is used in the display industry [1]. The process of determining the lifetime is shown in fig. 2. The curve shows the trend of the lumen maintenance for an LED up to the L70/L50 value. This can either be extrapolated or measured until total failure.

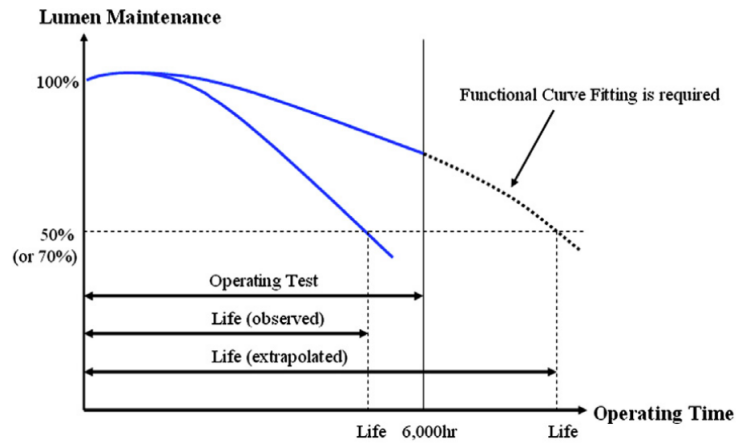


Figure 2: Lifetime estimation depending on the lumen maintenance, estimation can be done by observing or extrapolating L70/L50 value. [1]

Another way to determine the health state of an LED is to use temperature related parameters. In most cases, this can be accomplished much easier than light output measurements. Depending on the device temperature, measurements can be done directly via thermal sensors or indirectly using temperature dependent quantities. In the case of semiconductors, which have a temperature-voltage relationship, the voltage can be used as a reference. This enables very simple setups considering inline monitoring.

2.3 Network analysis via temperature transients

Using temperature-dependent parameters to estimate the health state of electronic devices is a popular method [20, 21, 5]. By defining a thermal resistance network for the device as a system of components, the temperature can be modelled even in more detail. Every component of the system can be described by its own thermal resistance which influences the heat transfer and its steady state operating temperature. This allows a precise analysis for failures at certain components. The formalism for a thermal resistance network model is equivalent to an electric circuit model. Temperature or voltage are potentials which follow the same calculation rules for these networks. Time-dependent temperature solutions can be obtained the same way, as time-dependent voltage signals from electric circuits/networks by using the impedance of the system.

There are a number of similarities between electrical and thermal quantities. Concepts such as flow, current or potentials occur in both areas and are essential for the characterization of the respective overall system. In table 1 some sizes are compared. The analogy of thermal and

electrical quantities can also be found in the formalisms. The equations for both thermal and electrical systems mathematically describe the same problem. The heat equation for thermal applications is similar to the form for Ohm's law. \vec{q} and \vec{j} denote the thermal flux and the current density, respectively. The other quantities like material constants and gradients are defined in table 1.

Table 1: Equivalence of electrical and thermal quantities

Electrical quantity		Thermal quantity	
Voltage	V	Temperature	T
Charge	q	Heat	Q
Current	I	Heat flow	\dot{Q}
Electrical conductivity	σ	Thermal conductivity	λ
Electrical resistance	R_{el}	Thermal resistance	R_{th}
Electrical capacitance	C_{el}	Thermal capacitance	C_{th}

$$\vec{q} = -\lambda \vec{\nabla} T \quad \text{Heat equation (Fourier law)} \quad (1)$$

$$\vec{j} = -\sigma \vec{\nabla} V \quad \text{Ohm's law} \quad (2)$$

For the consideration of temperature-sensitive parameters (TSEP), mainly temperature and heat flow or voltage and current are the relevant process variables. In electrical circuits, the behaviour of voltage and current over time is modelled using resistances and capacitances (or inductances). The impedance Z can be used to cast these two contributions in compact form. The impedance conveniently describes the relationship between current and voltage expanded for non-stationary states. In analogy, the temperature for thermal systems can be modelled using thermal resistances R and capacities C [22]. Since the system generally seeks for a state of equilibrium, the temperature equalization and thus the heat flow can be described via an RC network [23, 24].

Based on these analogies, the temperature changes can be modelled with the help of an RC network. The individual RC elements represent the layers in the system and are responsible for the evolution of the temperature over time [25, 26]. The aim is to determine these RC elements to be able to investigate the thermal process further. While the system is in steady state, the temperature is fixed at all locations, respectively the heat flow is constant. When performing a change in power (increase or loss) the temperature will also change, resulting in a dynamical process which seeks a new steady state. The stabilisation of temperature over time is called transient. The transient is the response to an “instantaneous” change, a step response to a sudden change in applied power, as illustrated in fig. 3.

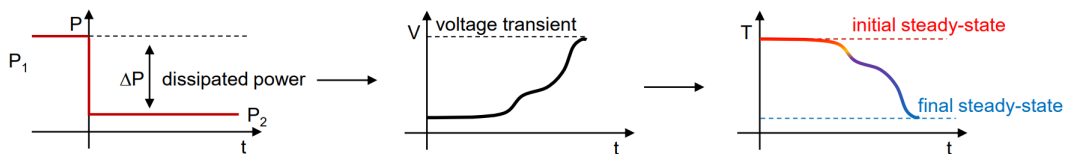


Figure 3: Transient as step response (process signal) due to instant change of control signal.

The behaviour of the temperature transient is determined by the RC elements. Therefore, the temperature transient can be used as a basis for calculating an RC network. The exact calculation of the RC elements is described in more detail in section 5.

Combining all these aspects, it is possible to use inline monitoring for failure and lifetime analysis. The monitoring can be done via temperature related parameters like the voltage signal for semiconductor devices, which is a perfect quantity for inline measurements. The RC network plays a central role as it associates changes in LED operation to certain locations in the LED and, hence, permits a detailed analysis of failures and other malfunctions. This forms the basis for all further monitoring actions.

3 Design under Test (DuT)

For the investigations exploiting inline monitoring, a four flip chip cluster LED module is used. Flip chip refers to an electronic component that can be mounted directly onto a substrate or carrier in a ‘face-down’ manner to e.g. enhance heat-dissipation efficiency of the LED. In fig. 4 the used PCB (printed circuit board) with two four-chip LED cluster, where always two chips are connected in series is shown. The PCB itself implements a copper core and a via structure on the back side to increase the heat dissipation. The flip chip LEDs can be contacted via the electrode pads, two per side. In table 2 the main parameters from the data sheet are summarized. The most important quantities are the maximum forward current and the maximum junction temperature, which should not be exceeded.

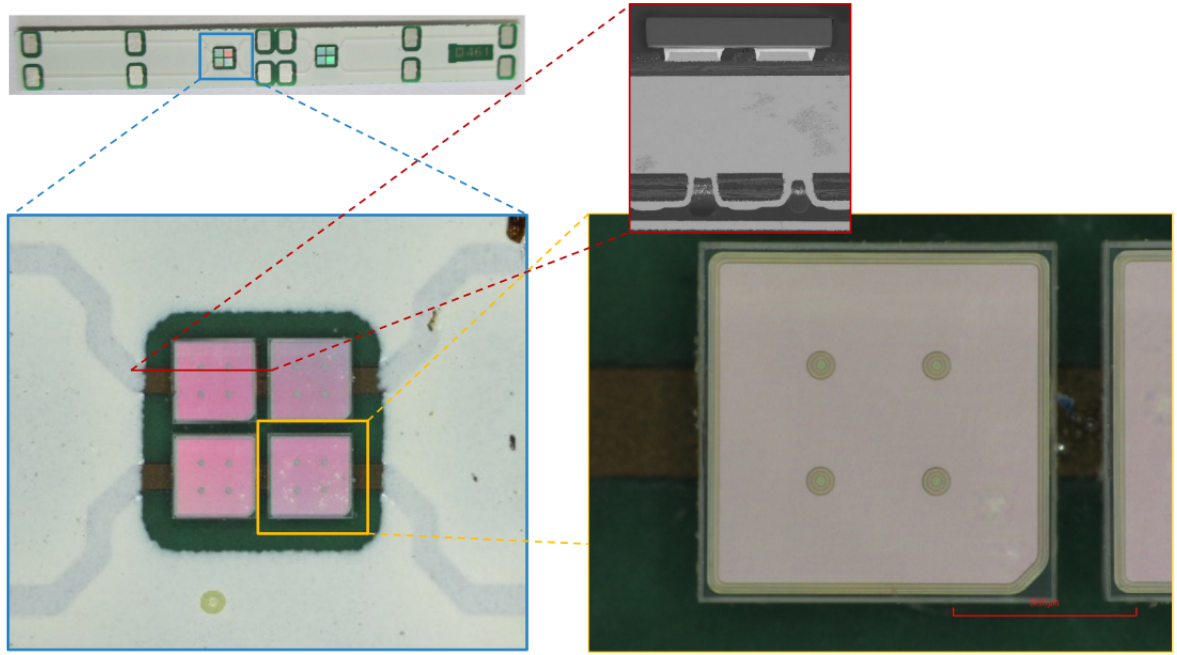


Figure 4: Pictures of LED modules with 8 flip chips EPistar mounted on a PCB. Four LED chip cluster (blue frame) with a detail view (yellow frame) of a single chip. Red frame shows an cross section from the chip, the two solder interconnection and the copper core based PCB with an via structure on the back side.

Table 2: Parameters for LED Chip EPistar Es-FADBPE38D [27], (T_a ambient temperature)

Parameter	Symbol	Condition	Value	Unit
Forward Voltage	Vf1	If = 10 μ A, T_a = 25 $^{\circ}$ C	≥ 1.6	V
	Vf2	If = 700 μ A, T_a = 25 $^{\circ}$ C	3.2-3.4	V
Reverse Current	Ir	If = 10 μ A, T_a = 25 $^{\circ}$ C	2.0	μ A
Dominant Wavelength	λ_d	Vr = 5 V, T_a = 25 $^{\circ}$ C	445-455	nm
Spectra Half-width	Δd	If = 700 μ A, T_a = 25 $^{\circ}$ C	25	nm
Forward DC Current	If	T_a = 25 $^{\circ}$ C	≤ 1000	mA
Reverse Voltage	Vr	T_a = 25 $^{\circ}$ C	≤ 5	V
Junction temperature	Tj	-	≤ 125	$^{\circ}$ C

For further measurements and testing, four PCBs are fixed on an aluminium plate with springs and wingnuts. The springs ensure an equal contact pressure for all boards and also allows to put

interface materials between board and plate. This is useful to have an influence of the heat flow.

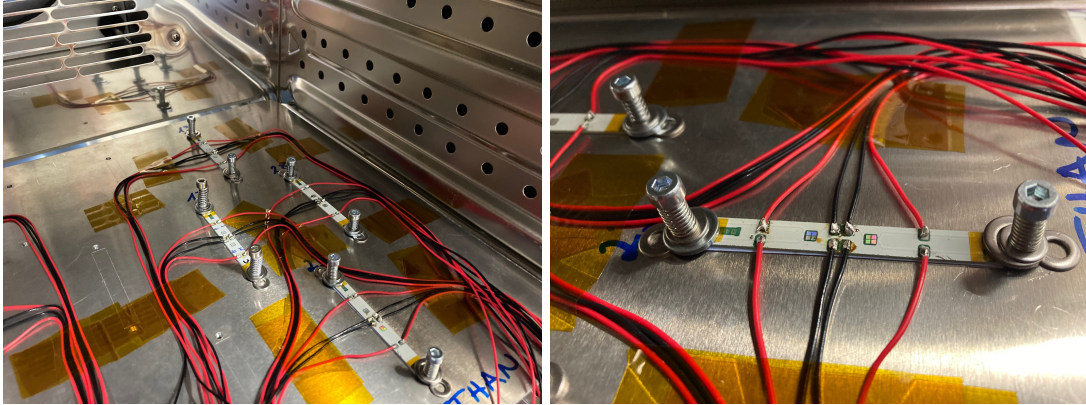


Figure 5: Setup of LEDs mounted on a PCB which is fixed with wingnuts and springs to ensure equal contact pressure.

3.1 Diode characteristics

As starting point, all LED chips were tested and verified for functionality. A simple on/off test and further a diode characteristic for single clusters (two chips in series) and double cluster (four chips in series) was recorded to see any deviations from each other. A KEITHLEY 2461 source meter was used to ramp the voltage level up to a maximum current of $I_{max} = 700 \text{ mA}$. These measurements were done three times in a row. All chips showed the expected diode characteristics, which is shown in fig. 6.

Voltage temperature characteristic

The temperature dependence of the forward voltage can be used to determine the ambient temperature via voltage measurements. To achieve this, one can simply put the boards in an oven in which the ambient temperature can be varied. The temperature range should roughly cover the values of the junction temperature under operating conditions. This guarantees a full characterisation of the voltage-temperature relation for the chips.

In fig. 6, you can see the diode characteristics at different temperatures. The range was chosen from room temperature to 80°C . The effect of the temperature is clearly visible, the forward voltage gets lower at constant current with increasing temperature.

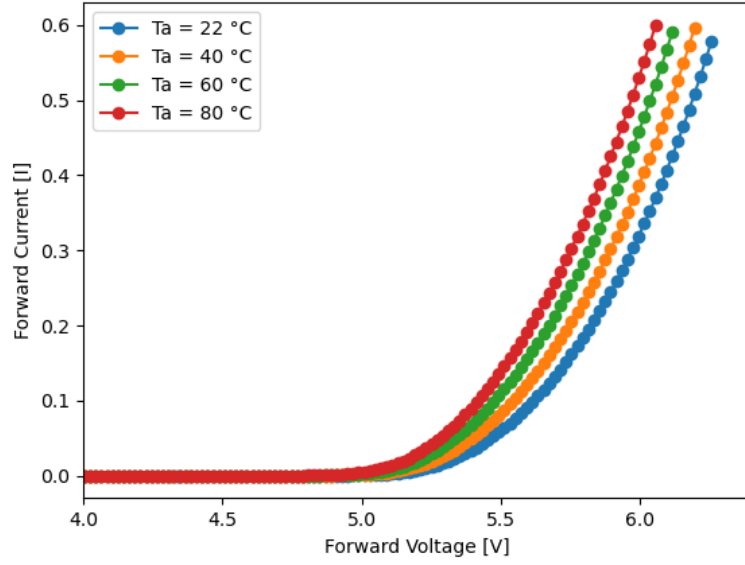


Figure 6: Diode characteristics for a single cluster at different ambient temperatures T_a , at constant current the forward voltage gets lower as the ambient temperature rises.

For a more precise calibration, the single clusters are powered at constant current during the whole heating process (temperatures 40 °C to 100 °C in 20 °C steps). The voltage is then measured with a REVPI AIO voltage meter [28], which allows a better evaluation for the temperature voltage relation. It also helps to find the steady state temperature which means the voltage level is constant at that time, see fig. 7.

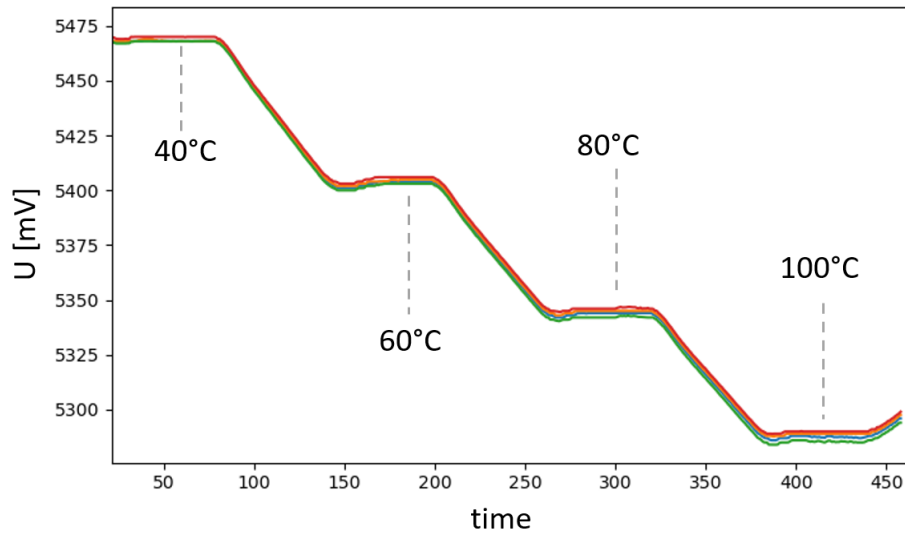


Figure 7: Monitoring of the voltage level at a constant measurement current. The plateaus represent the different temperature stages (temperatures 40 °C to 100 °C in 20 °C steps).

From this measurements, it is possible to evaluate the relation

$$U(T) = K \cdot T + T_0 \quad (3)$$

for all single clusters. The data is plotted for voltage over temperature and a linear function is assumed to provide a fit for the data points. In fig. 8 the measurements are plotted for a constant measurement current of 10 mA, 100 mA and 300 mA.

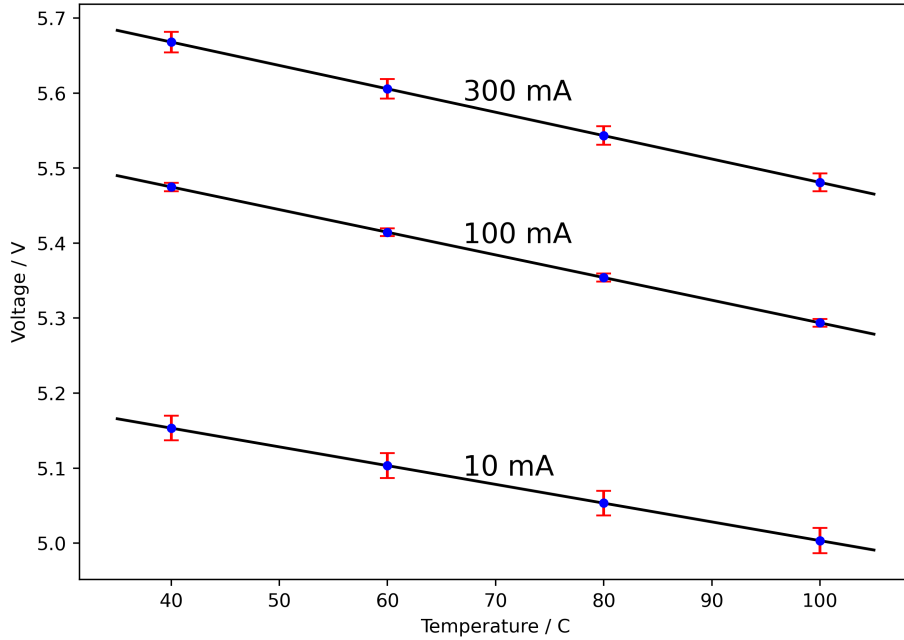


Figure 8: Measurement results, average voltage level at given oven temperature for different measurement currents (blue: 10 mA, orange: 100 mA and green: 300 mA). Black lines represent best fit through measurement data.

Different measurement currents were tested in order to find a minimal self heating current which still provides a voltage temperature relation. At minimal self heating, the junction temperature should approximately correspond to the ambient temperature. Then, the voltage level obtained at minimal self heating current represents the actual temperature of the device (respectively the junction). From the previous measurements 10 mA provided this condition and also a stable $U(T)$ relation. Therefore all further temperature measurements are based on this measurement current ($I_m = 10$ mA).

For every single cluster, there is a voltage-temperature measurement, therefore it is possible to compare the K values with each cluster to check if there is a unique relation or if one should use different values for each board. Figure 9 shows the distribution of the K values. Since all values form gauss curve and the standard deviation is rather small, it is legitimate to use the average of these K values for the $U(T)$ relation.

$$K = (-2.485 \pm 0.010) \cdot 10^{-3} \frac{\text{V}}{\text{K}} \quad (4)$$

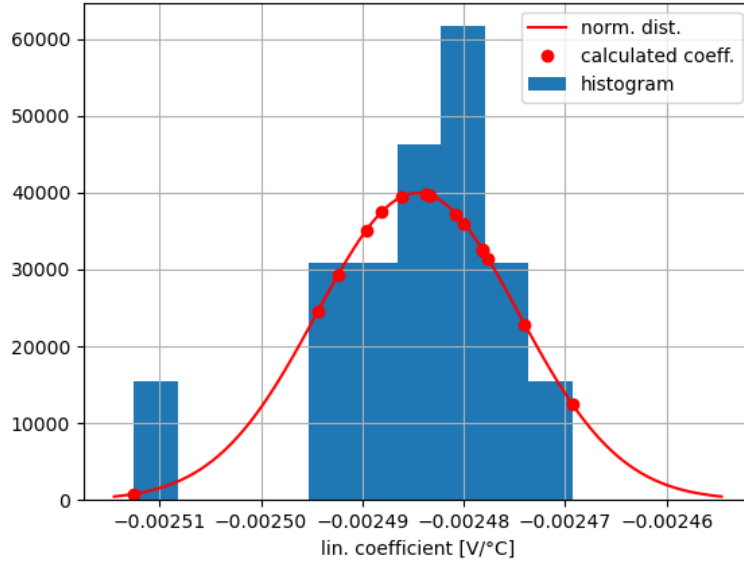


Figure 9: Statistical analysis of K values from the linear fits of the single cluster voltage temperature measurements

Derating

Derating curves basically give you information about the possible operation conditions of the device. Typically a LED is limited to some power or current value. If this limit is exceeded it can be harmful for the LED or, in a worst case, it gets destroyed. Though some limits are given from the data sheet of the LED, but there is a formally permitted range in which the maximum current would overheat the device. Therefore, the current has to be reduced to fulfil the temperature criteria.

For the EPISTAR LED, a derating curve was created via the limitations from the data sheet parameters in table 2. Additionally to this information it is necessary to know a relation for temperature and current for the LED, which is assumed like the following.

$$\Delta T \sim P \sim I^2 \quad (5)$$

The temperature difference of a LED is proportional to the dissipated power P which can be assumed to be quadratic in current. With this relation a derating curve can be plotted, as shown in fig. 10.

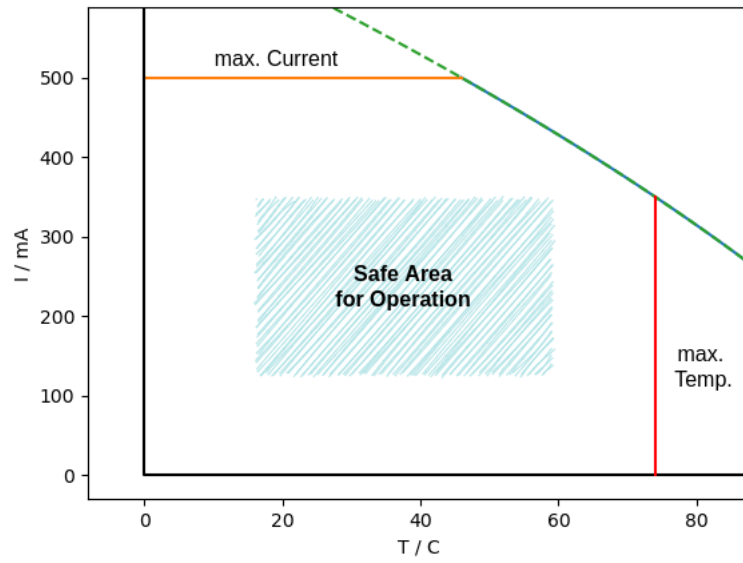


Figure 10: Derating curve of the EPISTAR LED showing the operation area, limited by maximal current and maximal temperature.

One of the advantages of derating curves is the quick overview of operation modes under full workload. For lifetime monitoring it is useful to stress the system with the maximal power, which can be found in the data sheets by derating curves.

4 TSEP measurement unit

The main principle of the measurement unit is to record the forward voltage as TSEP and evaluate the temperature via the $U(T)$ relation in section 3.1. The device also needs to measure the voltage level with a high sampling frequency in order to catch the cooling down process as a transient measurement of the LED. With these capabilities, it is possible to get further insight of the thermal processes.

4.1 Measurement device parameters

The portable sensing unit for TSEP measurements is an open source reconfigurable measurement instrument called RED PITAYA in combination with a daughter board called TT-Frontend developed at the MCL (Materials Center Leoben Forschung GmbH) [29].

The RED PITAYA, or STEMLab-board, is a small measurement board which contains hardware to do measurement tasks from common lab equipment. It is designed as small single-board computer with ARM processor, Field Programmable Gate Array (FPGA) and analog-digital/digital-analog converters [30, 31]. The RED PITAYA has many different functionalities, some common tasks are:

- Oscilloscope
- Function generator
- Spectrum analyser
- PIDs filters

The device provides access via network connection, which means measurements can be done via SSH connections or a web server. There is a wide range of open source programs available (applications) which can be used to control the hardware of the device. Since the operating system is Linux based, it is also possible to write own programs for special setups.

For this purpose of this master thesis, the STEMLab 125-14 (Red Pitaya v1.1) was used because it offers a 14 bits resolution for the input and output channels compared to the other board (STEMLab 125-10, 10 bits resolution).

Main properties [30] of Red Pitaya v1.1:

- 2 Fast Analog to Digital Converters, 125 MSamples/sec, 14 bits resolution, ± 1 V (or ± 20 V selectable by jumper settings)
- 2 Fast Digital to Analog Converters, 125 MSamples/sec, 14 bits resolution, ± 1 V
- Extension connector E1 for digital signals
 - 16 input/output 3.3 V digital signals that can be controlled by software or FPGA.
- Extension connector E2 for Slow Analog signals and other applications
- ARM based computer
 - Dual Core ARM cortex A9 processor
 - 4 Gb DDR3 SDRAM (512 MB)
 - MicroSD HD (up to 32 GB)
- FPGA: Xilinx Zynq 7010 SoC
- 1 Gbit Ethernet port for wired network
- 1 USB port

The TT-frontend (thermal transient frontend) is a digital voltage level shifter. It is controlled via a program from the Red Pitaya and shifts the incoming signal to a given offset voltage level. As mentioned previously, the Red Pitaya has two voltage ranges with 14 bits resolution. To get the highest resolution for the voltage transients, the smaller range ± 1 V is used. In most cases this range is enough to capture a full transient, therefore the offset voltage is compensated by the TT-frontend.

The TT-frontend is placed on top of the Red Pitaya case and output is directly connected to the Red Pitaya. The combination of the two parts as measurement unit is shown in fig. 11.

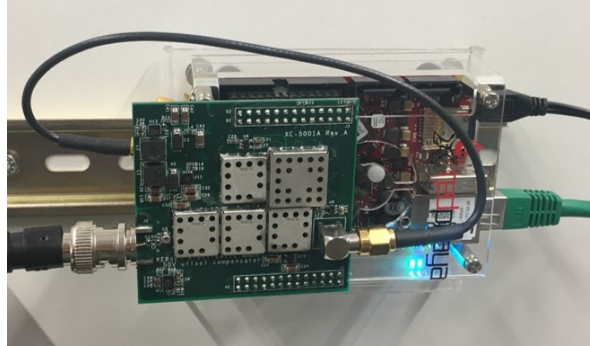


Figure 11: Measurement unit consisting of Red Pitaya and TT-frontend, the incoming signal is connected to the TT-frontend (green top board) which shifts the signal for a given offset voltage, the output is connected to the Red Pitaya (red bottom board) which performs the measurement.

4.2 Working principle

When running an LED with maximal power, the device heats up due to energy losses. It reaches a steady state temperature above the ambient temperature, which has influence on the electrical parameters. By reducing the applied power to the LED, more specifically, by setting a new constant current, also the temperature gets reduced. This results in a cooling down process. This changing temperature during the cooling down process affects the voltage level of the LED at a constant current. This voltage change caused by the thermal process of the LED can be recorded as a voltage transient. This transient basically results as a step response from the power supply, when the current is switched immediately to a lower level. At this point it is important to mention that power supplies have different switching rates and not all rates are fast enough to capture the pure thermal response without the noise from the power supply. Additionally, the lower current should fulfill the criteria of non-self-heating in order to relate the steady state temperature with the ambient temperature. At this current level also the K factor calibration is done which allows the mapping of the junction temperature $T_j(t)$ over time during the cooling down process.

With the Red Pitaya voltage signals can be recorded with high time resolutions. The setup for a transient measurement is shown in fig. 12. The LED is powered by the power supply at a constant high level current and has some high steady state temperature. Then a fast switching to a low measurement current is performed in order to allow the LED cooling down. During the whole process the signal is recorded by the measurement device. The voltage level of the LED is shifted by the TT-frontend such that the transient voltage lies in the range of ± 1 V. The output is connected to the input of the Red Pitaya and saved as $U(t)$ as bit values in a text file.

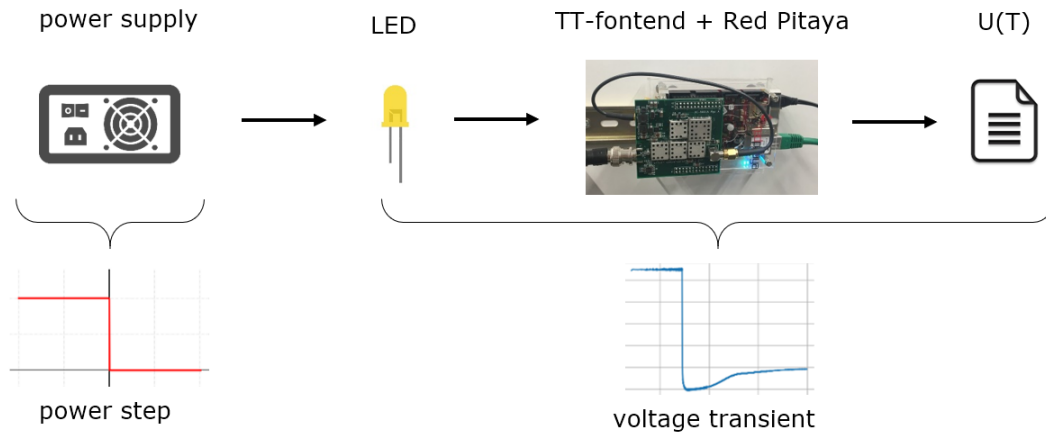


Figure 12: Working principle of measurement device, power supply does power step and switches to lower current level resulting in thermal transient which is recorded by measurement device.

In practice the measurement is started with a program from the Red Pitaya via SSH. It is customized for this purpose, such that the offset voltage with a range of ± 50 V and the time period for the measurements can be selected. The program now waits for drastic change in voltage e.g. a switch from the power supply and triggers the recording. An example of the execution command looks like the following.

Listing 1: Example command for starting a measurement at Red Pitaya

```
1 > ./tt_frontend 5.5 200 example_measurement_1
```

4.3 Trouble shooting

There are some issues which come along with the measurement device. Since the program for measuring a voltage signal is provided and changes cannot be done without further knowledge in the two components and the program language C, these issues are accepted. Some problems can be solved with some measurement tricks, others have to be accepted.

4.3.1 Time shift

The measurement device uses a buffer to save incoming voltage values in order to decide whether to trigger a falling edge or to continue waiting. This buffer when triggering is saved to the file and because the signal can randomly take place at any time, there is always a different starting point in time. This can lead to some problems if one has to know the switching point of the power supply accurately. Later on for calculating structure functions (see section 5) it is absolutely necessary for two transient measurements to have the same starting point for comparisons.

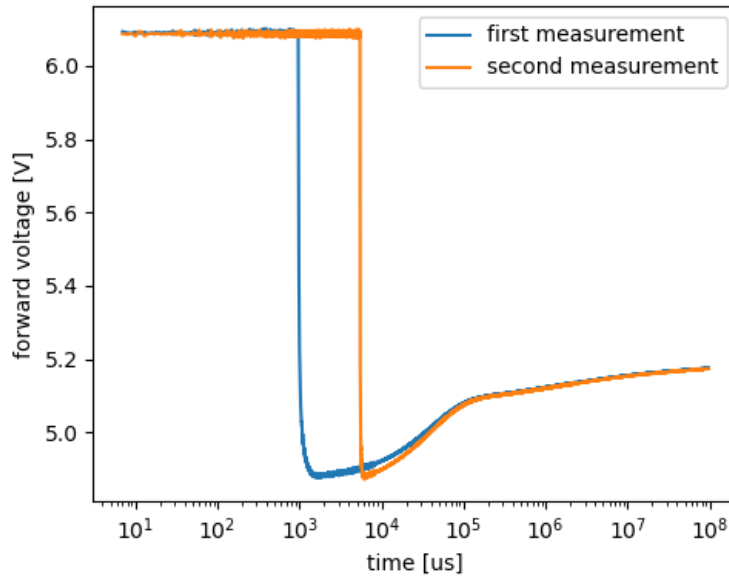


Figure 13: Example of two repeated measurements on the same LED with the same setup, the first measurement (blue) shows a significant time shift compared to the second measurement (orange).

This time shift can be avoided if both voltage levels, at load and at measurement current, are recorded. This guarantees that the falling edge is in the signal data and with this information the time can be adjusted. This method assumes that the voltage drop must lie in the range -1 V to 1 V in order to be able to measure the edge. Sometimes this may not be achieved and the measurements include some time shifts. In fig. 14 the time shifts for a sample of measurements are shown, the maximal deviation for two measurements is around 7 ms . Even if a time shift correction is done, some uncertainty for the time must be considered for further calculations.

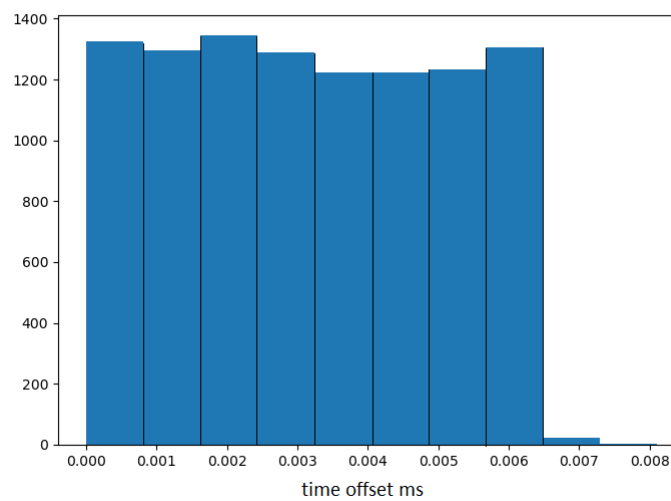


Figure 14: Time shift visualized, the time where the power supply switches is plotted in a histogram, the times are equally distributed since the start is random, maximal time shift 7 ms .

4.3.2 Data Points

The number of data points stands in correlation to the high sampling frequency. A high resolution in the first milliseconds is chosen to prevent information loss in that time range. This is a crucial aspect for analysis because there must be done a reduction of data points for computer calculations in reasonable time. Reduction can indicate information loss, therefore an algorithm which reduces the number of points and removes noise must be applied with some caution. In most cases a moving average combined with cluster averaging was done to the data, with respect to balance the number of points for analysis and the information content of the signal. For instance this means a measurement with 100 seconds containing 120.000 data points can be reduced to 1200 data points where the distance has logarithmic spacing.

4.3.3 Incorrect measurements

Sometimes measurements are invalid, that is, the recorded voltage transients show unexpected non-physical behaviour. This phenomenon is assumed to be related to the measurement device, since for different setups this phenomenon can be observed. For a single measurement a power supply, a LED, connection cables and the measurement device is needed. The invalid measurements can be reproduced with other independent power supplies, LEDs and cables, therefore the behaviour is related to the measurement device. In fig. 15, an incorrect measurement is shown. The main characteristic is the straight line and the sharp turn up to the steady state.

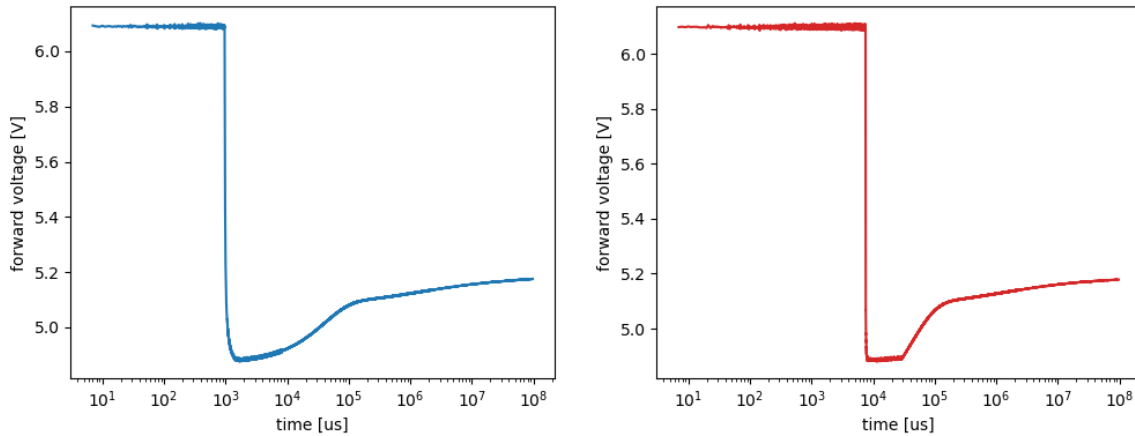


Figure 15: Comparison between a correct and incorrect measurement with the TSEP measurement device. Left a valid measurement which shows the voltage level as the LED cools down, right the same process but with invalid characteristics namely the straight line and the sharp turn.

There is no clear explanation for this behaviour, but it is supposed that the code which performs the measurements does not catch all possible outcomes and saves wrong data. During a long run experiment with many measurements a ratio of roughly 80% valid and 20% invalid measurement recordings was observed. This means a transient measurement should always be performed at least three times when it cannot immediately be checked by eye.

4.3.4 Time for measurements

The total measurement time for transient measurements must be chosen such that the temperature and, correlated to this, the forward voltage reaches a steady state. If the time is too short information from the transient is lost and the total thermal system cannot be fully reconstructed.

A longer time also means more data points and fewer transient measurements per minute, therefore the measurement time should be kept short as possible up to the point where still the whole transient is recorded.

The measurement device allows a maximum record time of around 5 minutes because of data overflow. This means the LED should be powered such that the transient process last below this limit. There is also the issue that the input time for the measurement program does not represent the real measurement time. The observed relation is that the measurement time is around half the input time. Since it is not known how the input time is used in the program this has to be checked for new measurements. To keep a constant setup for all measurement series the input time was fixed for all further measurements to 200 s (approx. 96 s real time).

5 Processing with structure functions

5.1 Structure function as a tool

The structure function is a useful tool for analysing the thermal resistances obtaining from an one-dimensional heat path [32]. The associated thermal resistance profile supports a detailed analysis for the structure of the system and further its behaviour under thermal changes.

The principle of the structure function is based on the decomposition of the step response from a sudden power change to the diode. If the power is reduced, the diode will cool down as less power is lost in the form of dissipation heat. This cooling process becomes visible as a temperature transient at the junction (location of the heat source) and can be viewed as a heat transfer to the environment along a one-dimensional but not necessary straight path. To calculate the structure function, this temperature transient is decomposed to a group of RC elements representing a thermal network. This network can explain the cooling down behaviour of the device. The procedure is similar to analyzing an electrical RC network (thermal resistances and capacitances) and can in principle also be used for current and voltage. However, structure functions are mainly used in thermal processes and are used to model the heat path through the system.

With the help of the structure function it is possible to examine structures of the system more closely. The interpretation of the structure function makes a variety of applications possible: Functional layers in the system (diode, connection, PCB, heat sink, etc.) can be related to thermal resistances. Layer boundaries, at least in rough form, can be possibly identified. More detailed layers can be reduced by simulating the heat path [33]. Based on the knowledge of the layer boundaries, it is possible to make an analysis of possible sources of failure for the system itself in the form of low heat conductivity. Potential sources of failure are large thermal resistances, which can overheat the system. This has an adverse effect on the life time of the device and is an important aspect for practical applications.

A prominent point of applications is the monitoring of thermal resistance. The structure function can be calculated for the device at different times to determine whether there is a change in the thermal resistance. The change in thermal resistance can be interpreted in different ways. Nevertheless mainly long-term failures or mechanical effects are linked to it. Aspects to lifetime and failure rates are discussed in section 2, further information on the service life can be found in [15, 34].

5.2 Computation steps of the structure function

For calculating the structure function some requirements are given. The calculation of the structure function should be possible “inline”, that is it runs parallel to the measurement cycle (see section 7). Therefore the calculation time must not take longer than a single measurement cycle. In addition, it makes sense to carry out the calculation in PYTHON, since it can be evaluated directly on the measuring device if necessary. This makes the measuring device even more powerful and compact for determining life time and ageing processes. The following subsections describe in detail the single steps of the calculation procedure, which are necessary for obtaining the structure function, or respectively its RC network. Time constraint required a new implementation of the evolution originally proposed by L. Mitterhuber [32].

5.2.1 Preparation

At the beginning, the raw data must be prepared. The measurement device records voltage transients with high resolution and saves them in a text file with time values and bit values for

the voltage. An example of the file can be seen in listing 2. The first lines of the file contain the values for the offset and the LSB (least significant bit) for converting the voltage values.

$$U_{\text{volt}} = U_{\text{bit}} \cdot \text{LSB} + \text{Offset} \quad (6)$$

Listing 2: File structure of a transient measurement with the Red Pitaya

```

1 # *MCL LED-TT* TIME RESPONSE RECORD
2 # [17 11 2018 17:20:19]
3 # 819216382201 //Running Experiment number
4 #
5 # Offset Voltage: 5.0000000
6 #
7 # 1.4404e-004 LSB Voltage Equivalent
8 #
9 #
10 # 81920 //No. of Samples
11 7 3415
12 8 3443
13 9 3333
14 10 3396
15 11 3399
16 12 3428
17 13 3378
18 14 3380
19 ...
20 ...

```

After calculating the voltage values in volts, the parameters $U(T) = K \cdot T + U_0$ must be specified for the conversion into temperature values. These are determined by calibrating the device and remain the same for the whole series of measurements. The third parameter ΔP is the change in power when switching to the measurement current. This is determined separately for all measurements and does not necessarily need to be specified.

$$\Delta P = U_{\text{heat,stable}} \cdot I_{\text{heat,stable}} \quad (7)$$

Since the measurements do not all start at the same point in time (see Time shift section 4.3.1), the data points have to be adjusted in time. The time at which a measurement starts is determined via the falling edge. The point in time with the steepest slope is used as a measure to compare two measurements. This step is absolutely necessary for the measurement recordings with the TSEP measuring device, but can be ignored for other recordings without time shift.

One problem that was already noted in section 4.3.2 is the number of data points in the file. The number is a fixed parameter by the measurement device, so it must be checked, whether a reduction is necessary. One big advantage of a reduction is the smoothing of the signal, which is recommended for a more stable result. The 'Cluster-Average' function is used for the reduction, whereby a cluster of points is combined to form an average. This allows the number of points to be reduced significantly, and the curve also gets smoothed. In order to reduce the noise even further, a 'moving average' can be used, which averages the points in a given window but does not reduce them any further.

The parameters for the reduction and smoothing of the transient measurements should be set and checked for every new measurement series. The program itself does not work with optimal

parameters since there is no evaluation and must be set by the user.

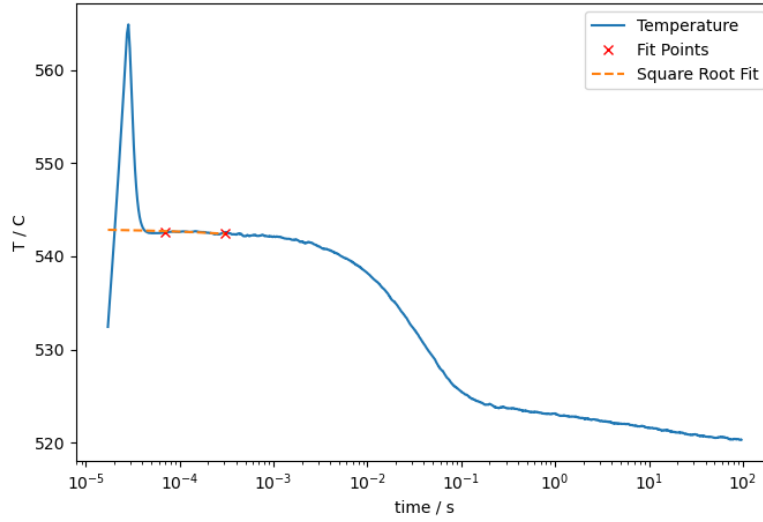


Figure 16: Fit point range (red crosses) for square root fit of $T(t = 0)$ to remove the electrical noise from the power supply. (Note that the absolute temperature values does not match with real values since the offset is not chosen properly.)

The last parameter to be specified is the range for the square root fit. This time range is already applied to the smooth temperature transient, therefore set last. It should be checked visually whether the range has been selected appropriately so that the temperature $T(t = 0)$ is correctly determined. In some cases, especially with a large series of measurements, it can happen that the fit range has not been set optimal. This can have great impact to the calculation process of the structure function. It is recommended to check all calculations visually for a small series of measurements and to check random samples for a large number of files. Nevertheless, errors in the evaluation of the structure function can occur in the case of irregular input files.

5.2.2 Calculation

In this chapter the single steps for calculating the structure function are briefly introduced. Starting with the prepared temperature transient including the smoothing and the square root fit, it is used as input for the calculation algorithm. In fig. 17 the compact computation process is shown. It starts with the temperature transient, which is transformed over four intermediate calculation steps to the Cauer network, which represents the structure function.

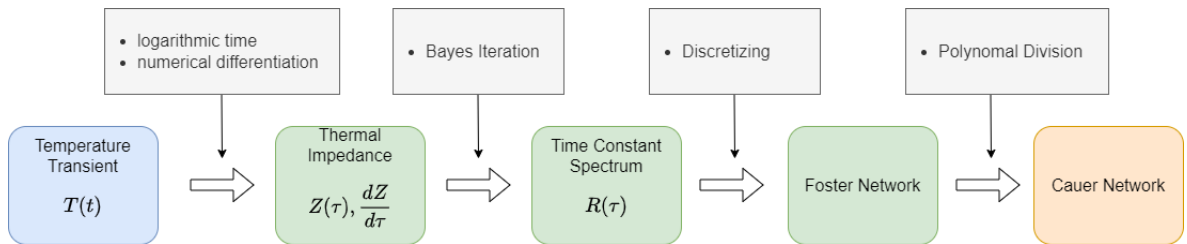


Figure 17: Computation process of the structure function.

First step is the determination of the thermal impedance Z . It represents the temperature evolution over time and is dependent on the efficiency with which heat is transferred to the

surrounding. For the calculation of the thermal impedance, the temperature transient is used, which arises when the applied power on a device changes. Thermal transient measurements are based on the electrical test method, which procedures are defined in references [35, 36]. The second step is the numerical deconvolution via Bayes iteration to generate the time-constant spectrum. Discretization (third step) of the time-constant spectrum results in a Foster network for the continuously distributed case. The Foster model network is just a theoretical representation of the time constant spectrum and does not correspond to the physical structure of the thermal system, since the thermal capacitance exists towards the ambient (thermal “ground”) only. Therefore step four is to convert the model network into the Cauer network, as shown in fig. 18.

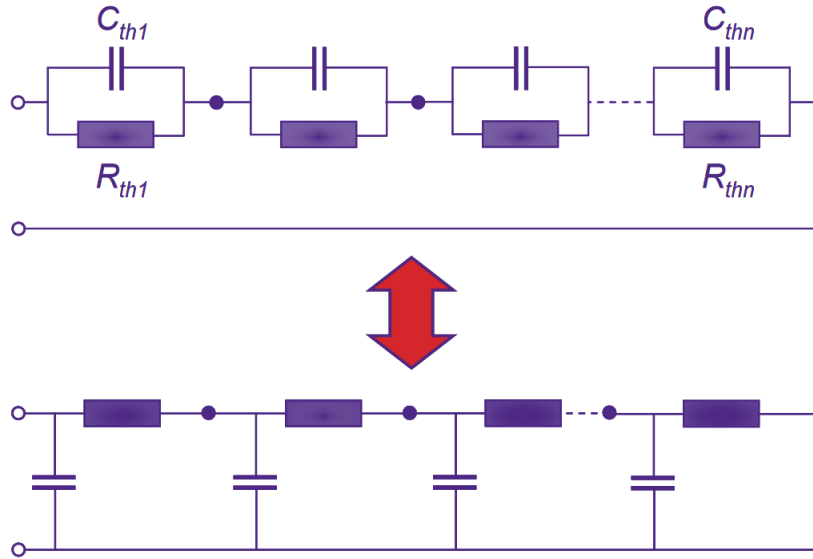


Figure 18: Foster network (above) and Cauer network (below) as byproducts of the calculation process [36]. R_{th} and C_{th} describing the thermal resistances and capacitances in the network.

The identified RC model network in the Cauer canonic form now corresponds to the physical structure. Its graphical representation (see fig. 19 and eq. (8)) is called cumulative structure function and represents the map of the heat-conduction path from the junction to the ambient. Plateaus correspond to a certain material and the volumetric thermal capacitance can be read out.

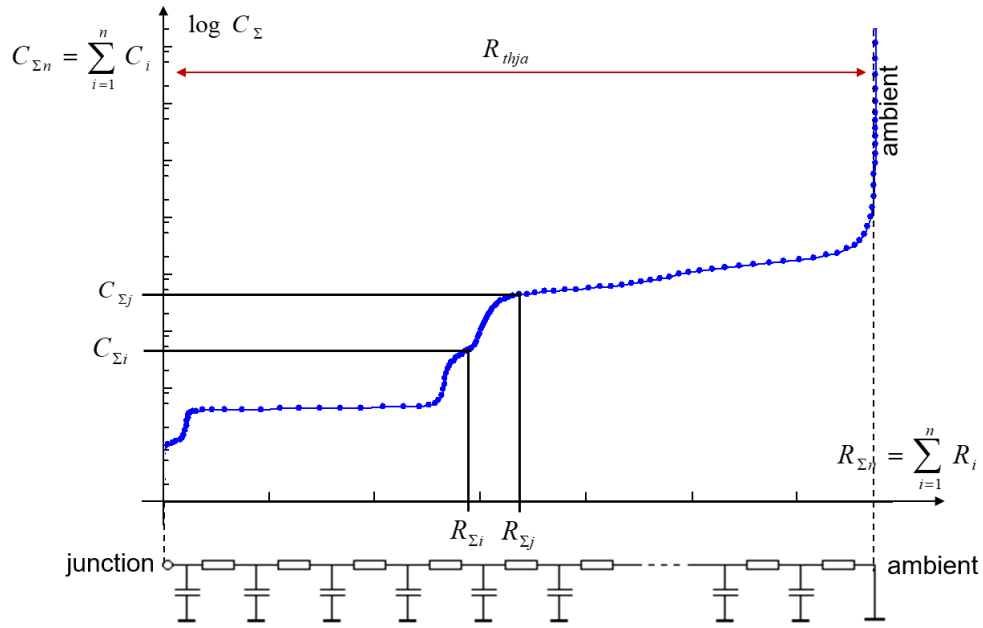


Figure 19: Structure function from the Cauer network representation.

The RC network can also be presented by the differential structure function, which is defined as the derivative of the cumulative thermal capacitance with respect to the cumulative thermal resistance (eq. (9)) and is proportional to the square of the cross section area of the heat flow path.

$$C_{\Sigma,i}(R_{\Sigma,i}) := \left(\sum_{j=1}^i R_j^C, \sum_{j=1}^i C_j^C \right) \quad (8)$$

$$\frac{dC_{\Sigma,i}}{dR_{\Sigma,i}} \rightarrow \frac{\Delta C_{\Sigma,i}(R_{\Sigma,i})}{\Delta R_{\Sigma,i}} \quad (9)$$

The complete calculation process can be found in further detail in [36], where the test method standard is explained and in [32] where thermal behaviour analysis is described.

5.3 Benchmarking

The performance of the code for the calculation of the structure function is now to be evaluated. Two criteria are important for the evaluation. The first criterion is the quality of the calculation. The end result and also the intermediate steps should agree with other process systems that such as the T3STER Master. The calculation should also be independent of the measured temperature transient in order to work with other measurements next to the Red Pitaya as well. The second criterion is the time in which a complete calculation of the structure function is possible. This is an important parameter, since the duration of cycle measurements must be longer than the calculation time in order to enable inline monitoring. In addition to these criteria, the influence of the input parameters is examined. Sensitive parameters can drastically change the evaluation of the structure function. Therefore, it is useful to know the deviation of the structure function for small changes in the input.

5.3.1 Validation with different systems

During the development of the program for calculating the structure function it has already shown that small deviations in the results are unavoidable. The deviations are originate from various sources, like parameter settings for the fit and calculation steps or whether to the T3ster rather than the Red Pitaya is used for acquisition. An exact mapping with the same input values is therefore not possible. To compare two structure functions, a visual check is suitable to determine whether there are distinctive sections. Attention is paid to the number of R_{th}/C_{th} steps and R_{th} peaks respectively. For the quantitative check, the thermal resistance of the entire system is taken as reference. The total thermal resistances $R_{th,A}$, $R_{th,B}$ from two different structure functions A and B (which describe the same system) is used to calculate the relative difference $\Delta R_{th,rel}$.

$$\Delta R_{th,rel} = \frac{R_{th,A} - R_{th,B}}{R_{th,B}} \quad (10)$$

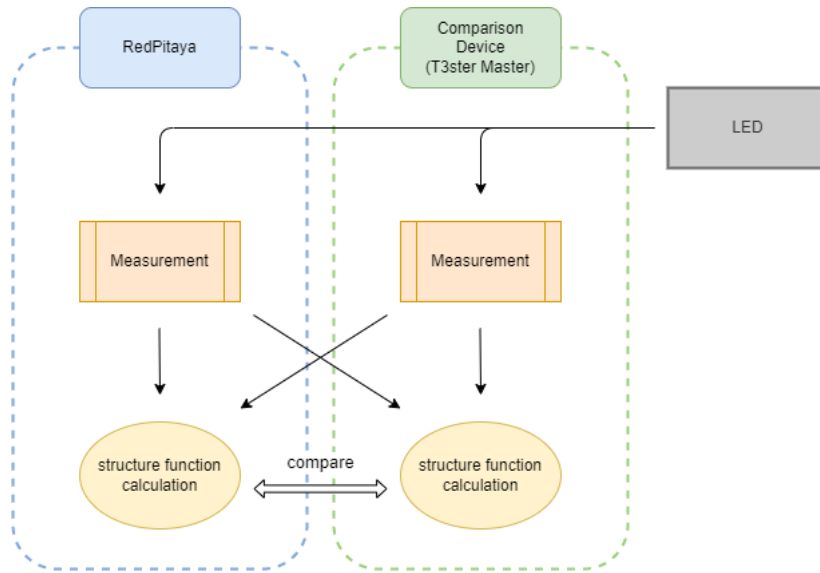


Figure 20: Workflow for comparing two separate structure function evaluation systems. The systems contain its own measurement operation and calculation operation. Left Red Pitaya as a compact system, right comparison device respectively the T3ster Master

In fig. 20 the evaluation paths to compare the final structure function are shown. The main device to quantify is the Red Pitaya and the comparison device is the T3ster Master. Basically there are three possible combinations to check.

1. **Comparison with T3ster measurement**
Comparison: Calculation newly implemented Code vs. Calculation T3ster
2. **Comparison with Red Pitaya measurement**
Comparison: Calculation newly implemented Code vs. Calculation T3ster
3. **Processing with Red Pitaya vs. Processing with T3ster**
Comparison: Evaluation of the structure function for two complete separate process systems

Comparison with T3ster measurement

The first comparison guarantees the correct calculation of the structure function with a temperature transient provided by the T3ster system. The remaining free parameters of the calculation,

like K-value, power step and time shift, were set optimal so that the smallest possible deviation from the reference (T3ster transient measurement) is given.

Figure 21 shows the quantitative comparison between the Red Pitaya and the T3ster calculation. A measurement series of voltage transients was recorded by the T3ster Master and the total thermal resistances for the device were calculated. One can see that most values are centered near zero, so the calculations match with the total thermal resistance. However the structure functions can still show different intersections for the LED, that's why a further visual check of the peaks is needed.

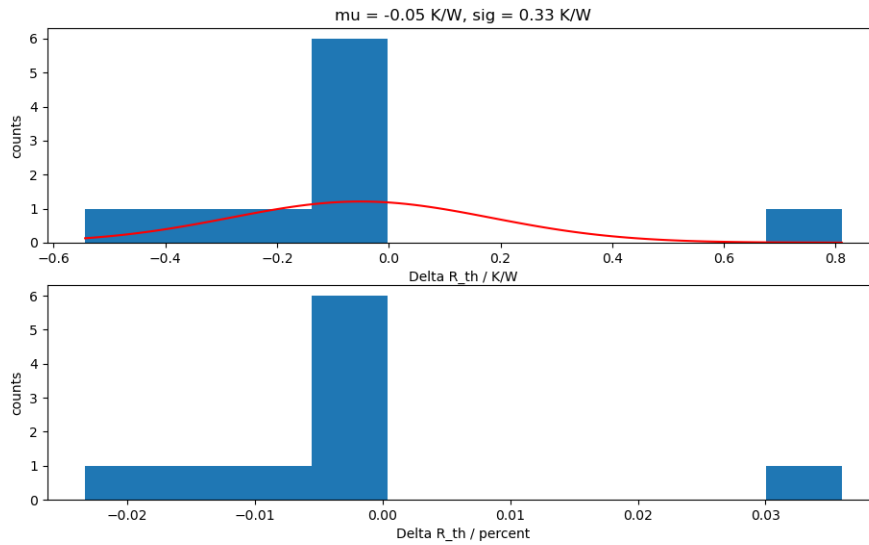


Figure 21: Histogram of thermal resistances obtained for different T3ster measurements, above absolute difference, below relative difference. The mean deviation ΔR_{th} is found at -0.05 K/W .

In fig. 22, the structure function and the derivation for a transient measurement with 200 mA heating current and 10 mA measurement current can be seen, whereby a cooling time of 100 s was used. It can be seen that the structure function and also the differential structure function show some deviation to the reference. The calculation routines of the T3ster software are not shown in detail to the user. Different preparation steps can change the input for the calculation which can lead to different results with other structures. However, the most peaks for higher thermal resistances are present, which is sufficient to describe the structure function and its thermal heat path.

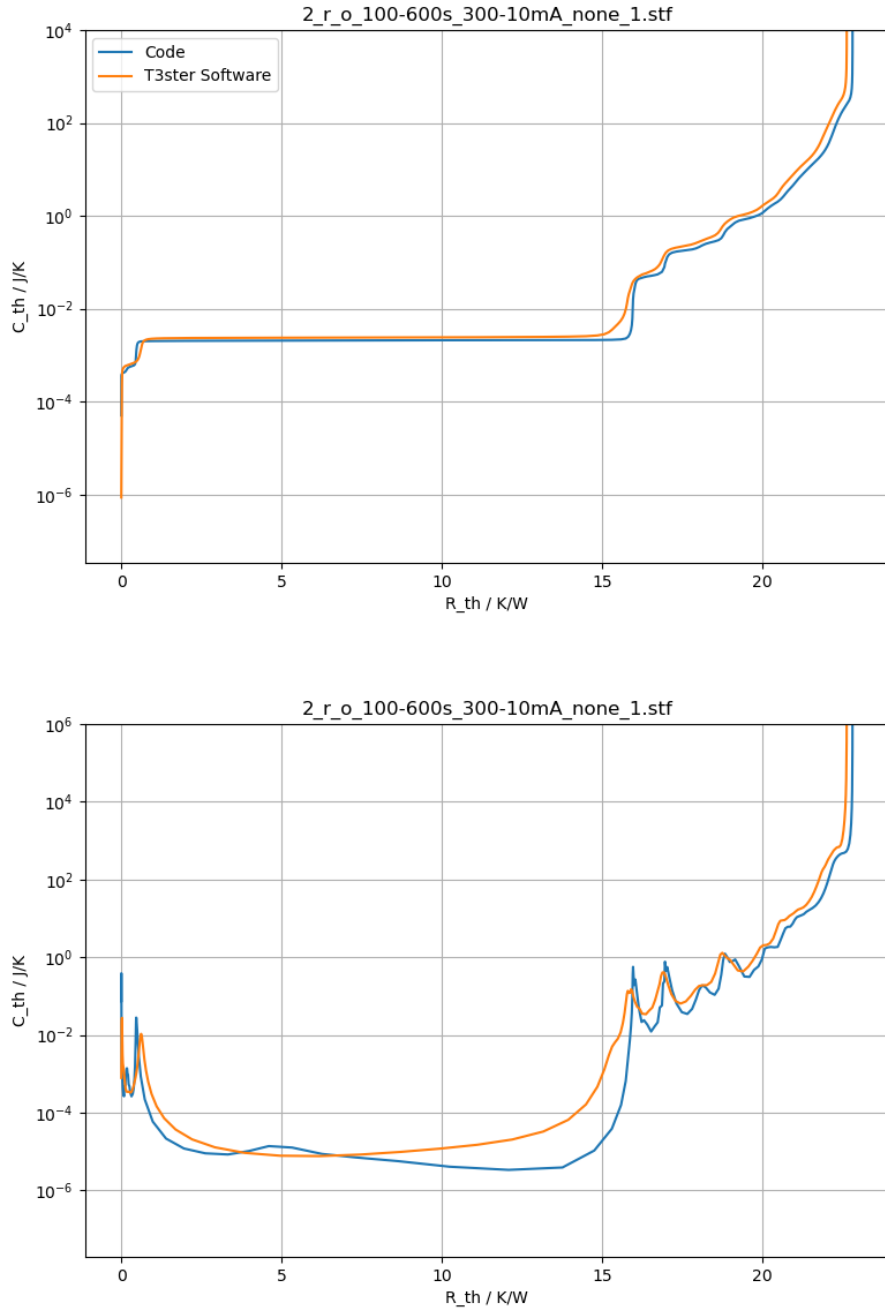


Figure 22: Structure functions calculated by the Red Pitaya and the T3ster Master from prerecorded measurement data from the T3ster. Top figure shows the cumulated structure function, bottom figure shows the differential structure function.

Comparison with Red Pitaya measurement

The second comparison is done to ensure that measurements with the Red Pitaya are done correctly and prepared adequately for the calculation of the structure function. For this purpose, measurements from the Red Pitaya are used and evaluated with the T3ster Master software and with the newly implemented Python program to obtain the structure functions. As already mentioned, the Red Pitaya measurements have a time shift due to the measuring device. This is not corrected for the comparison, since no such correction known takes place in the calculation

of the T3ster Master. Since only the calculations are compared, this step is legitimate, but the results are distorted from the real values.

First a measurement series of voltage transients was done with the Red Pitaya. The structure functions were calculated for each measurement with the Code and the T3ster software. From this the total thermal resistances were taken to calculate the relative differences via eq. (10), which is shown in fig. 24. The deviation was estimated by fitting the data points with a normal distribution.

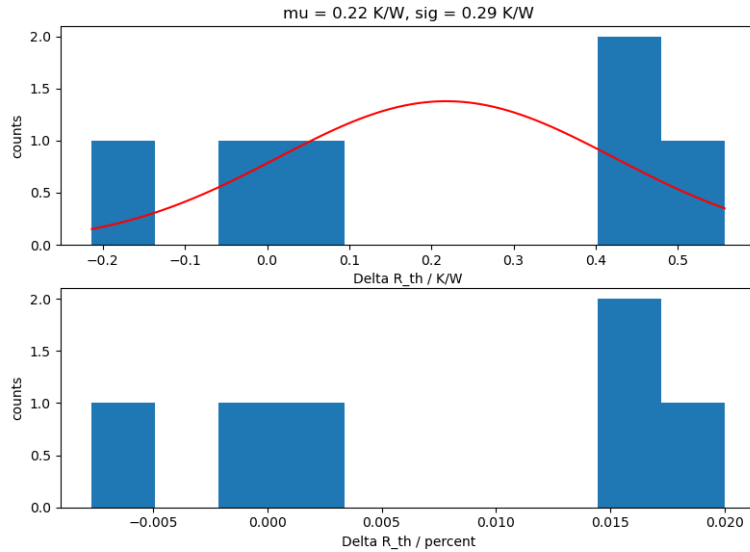


Figure 23: Histogram thermal resistances for different Red Pitaya measurements, above absolute difference, below relative difference. The mean deviation ΔR_{th} is found at -0.22 K/W.

The evaluation of a measurement can be seen in fig. 24 (heating current 400 mA, measurement current 10 mA). It can be seen that the total thermal resistance is quite the same. The peaks are the same for large resistances, but there are deviations for small values. One possible cause for the latter deviations is the time shift, which was not corrected. The T3ster's routine for such cases is not exactly known.

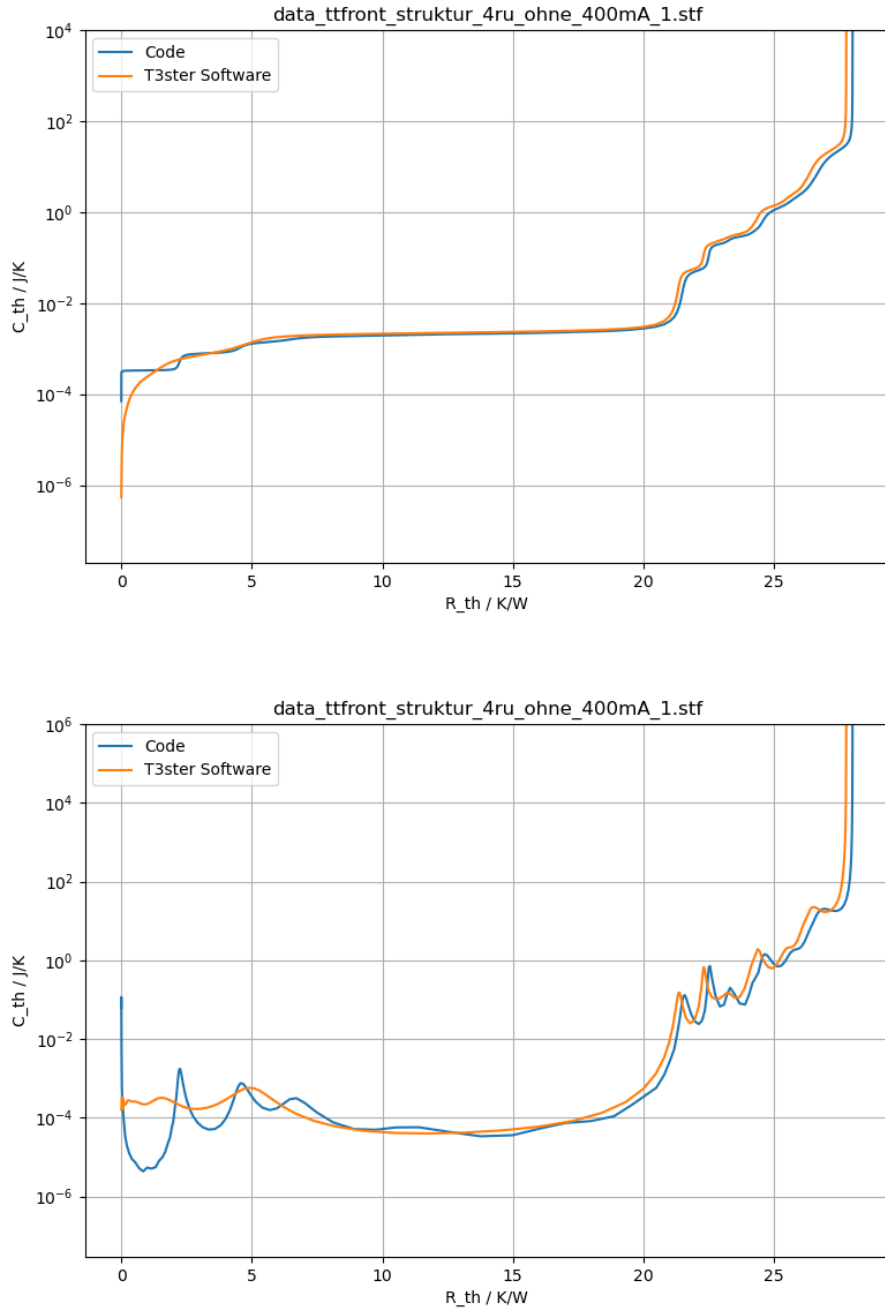


Figure 24: Structure function evaluation for TSEP measurement, main peaks match with reference calculation, deviations are present for small values.

Comparison with separate Red Pitaya and T3ster measurements

The third comparison evaluates the results from two independent measurements and calculations. Both measuring systems should come to the same result after the same measurement and evaluation, so that the structural function can be reproduced. For the comparison, a Red Pitaya measurement and a T3ster measurement were made under the same conditions for the LED. It was found that the Red Pitaya measurement was shifted by 8 ms (compare section 4.3.1) to the T3ster measurement. The voltage signal was also constantly shifted by 1.38 V to each other because of different cable setup. The deviations are acceptable in the context of the calculations

and have been corrected. Also the recording time is not the same. The Red Pitaya recording time is smaller than the set value (compare section 4.3.4). This is still valid since the temperature value is in an equilibrium. The recorded transients can be seen in fig. 25.

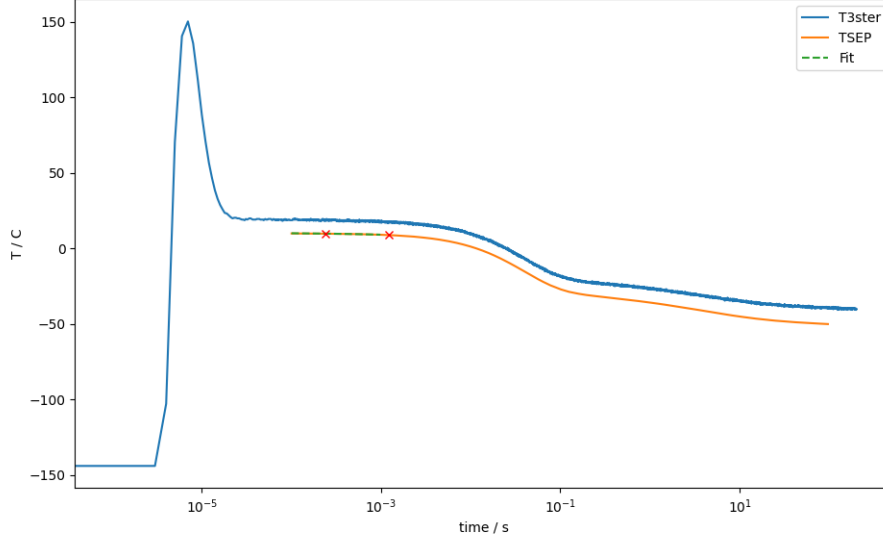


Figure 25: Separate temperature measurements with T3ster and TSEP. TSEP curve shifted by an temperature offset of 8 K for visualisation. The calculation process uses temperature differences, therefore the y-axis does not show the absolute values, all temperature values have a constant offset. Red crosses with green dotted line representing the fit for T_0 .

The comparison for the two structure functions is shown in fig. 26. For the differential structure functions most of the peaks match, but there are deviations for small resistance values ($R_{th} < 7 \text{ K/W}$). Both total thermal resistances agree each other within a uncertainty of 0.5 K/W .

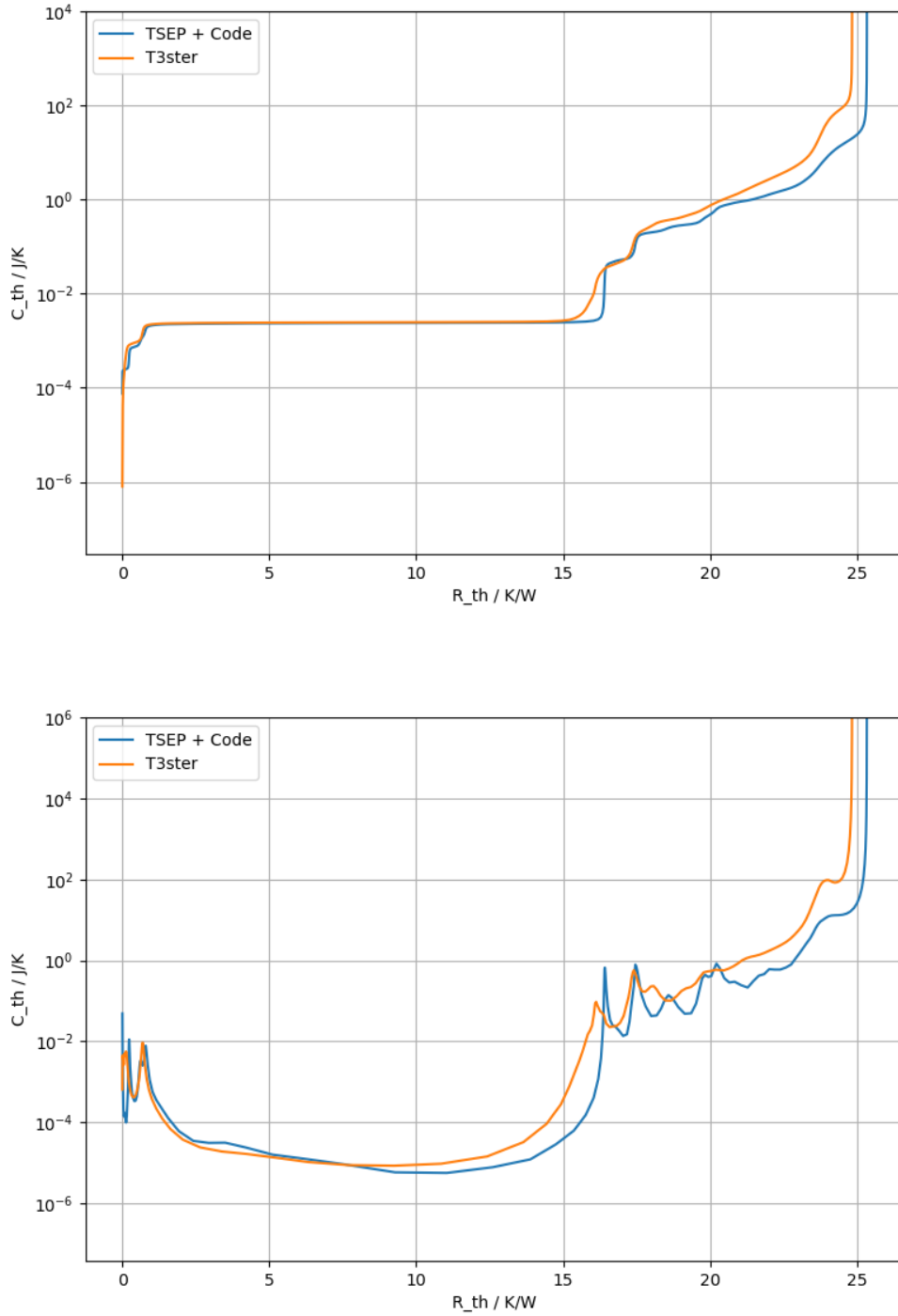


Figure 26: Structure function evaluation for TSEP measurement and T3ster measurement separately. Small deviations for some peaks, total thermal resistance match with 0.5 K/W.

5.3.2 Time and CPU consumption

The profiler in SPYDER is used to test the runtime of the code. A complete calculation of the structure function is called once for a Red Pitaya measurement. The execution sequence is as follows:

1. Read file and calculate U and t (*readRedpitaya*)
2. Create class of structure function (*init*)
3. Set input parameters (*setParams*)
4. Perform cluster average (*averageCluster*)
5. Perform moving average (*averageMoving*)
6. Create square root fit (*setFitPoints*)
7. Calculate all quantities including structure function (*calculate*)
8. Plot structure function (*plot*)

In fig. 27 the times for the individual calculation steps are sorted according to the total time. The duration of the test function *testing*, which contains all calculation steps, is approx. 900 ms. You can see that most of the time (approx. 500 ms) is spent on calculating the structure function (*calculate*). Here some sub-calculation steps are included, which are called several times. The time is mainly dominated by the functions *Cauer* (calculation of the Cauer network via polynomial division, 190 ms), *Bayes2* (Bayes iteration to calculate the time constant spectrum, 170 ms) and *NomDenom* (creation of the polynomials for the transformation of the networks, 110 ms) together. In addition to the calculation, reading in the file (130 ms) also takes a long time compared to the total time. This can be a matter if many files are needed to be evaluated immediately. The remaining functions are negligible over time. Plotting the function does not have to be done immediately every time and can be skipped.

Function/Module	Total Time	Diff	Local Time	Diff	Calls	Diff
find_and_load	1.26 sec		9.23 ms		752	
testing	909.23 ms		10.01 ms		1	
calculate	494.32 ms		233.40 ms		1	
Cauer	189.66 ms		20.03 ms		1	
Bayes2	169.95 ms		14.51 ms		1	
fft	92.70 ms		2.28 ms		3002	
ifft	62.74 ms		1.58 ms		2001	
<built-in method builtins.len>	11.61 ms		10.63 ms		101931	
<method 'copy' of 'numpy.ndarray' o.	298.20 us		298.20 us		205	
<method 'argmin' of 'numpy.ndarray' o.	3.90 us		3.90 us		1	
NomDenom	109.30 ms		6.02 ms		1	
__init__	22.48 ms		22.37 ms		1	
diff	2.03 ms		67.50 us		40	
polyfit	1.09 ms		2.70 us		1	
doRCvalues	705.60 us		565.50 us		1	
_showwarnmsg	556.80 us		2.10 us		1	
<method 'argmax' of 'numpy.ndarray' ob	396.40 us		396.40 us		3	
<method 'copy' of 'numpy.ndarray' objec	298.20 us		298.20 us		205	
<method 'cumsum' of 'numpy.ndarray' o.	137.80 us		137.80 us		9	
logspace	123.70 us		2.60 us		1	
<method 'max' of 'numpy.ndarray' objec	61.40 us		9.10 us		6	
__call__	56.50 us		4.70 us		1	
polyval	47.80 us		2.20 us		1	
__init__	4.80 us		4.80 us		1	
averageCluster	159.47 ms		1.60 ms		1	
cluster_average	157.88 ms		8.41 ms		2	
mean	104.30 ms		6.27 ms		9468	
array_split	45.15 ms		7.40 us		2	
<built-in method builtins.len>	11.61 ms		10.63 ms		101931	
<built-in method numpy.zeros>	617.60 us		617.60 us		203	
readRedpitaya	126.53 ms		1.58 ms		1	
setFitPoints	75.81 ms		120.30 us		1	
figure	62.50 ms		58.20 us		2	
plot	22.12 ms		26.20 us		1	
timeShift	6.52 ms		4.68 ms		1	
setParams	1.79 ms		1.79 ms		1	
__init__	1.32 ms		1.32 ms		1	
averageMoving	181.60 us		6.30 us		1	
_handle_fromlist	813.19 ms		3.21 ms		3497	
close	970.00 us		29.40 us		8	

Figure 27: Results from profiling the code with one full calculation. Total time 1.26 s.

With approx. 1 s, the time for calculating the structure function is well suited for inline monitoring. Typical times for transient measurements are >10 s. Depending on the intended use, the computer

memory should also be taken into account if many files are read in. It is recommended to save the structure function and to release the memory again. The input file should also not be too large. Files containing a great number of data points slow down the calculation and unnecessary stress the measurement/calculation unit while operating.

5.3.3 Error estimation of parameters

When evaluating a series of measurements, input data or individual parameters can vary. However, the uncertainty of these variables must be small enough to prevent a change in the evaluated structure function. In order to test the effects and the influence for individual parameters on the structure function, the calculation is performed for slight changes of the input parameters. The total thermal resistance is the measure to evaluate the influence of parameter variations.

The most important input parameters for the calculation of the structure function are:

- time shift of measurement device
- K-factor for $U(T)$ relation
- dissipated power ΔP

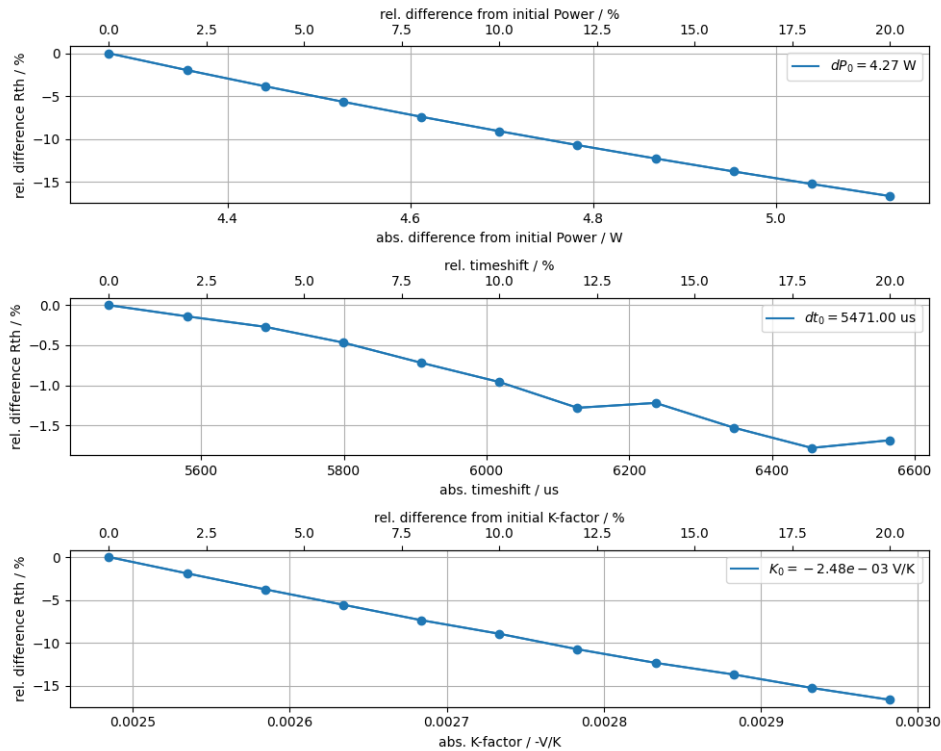


Figure 28: Variation of input parameters. From top: dissipated power ΔP , time shift Δt and temperature-voltage relation factor K .

The influences of the individual parameters can be seen in fig. 28. It turns out that the power and the K factor have the same influence on the thermal resistance, since both directly enter the calculation for the thermal impedance as factors. They are also the most influential parameters and must therefore be carefully determined. The time shift has less effect on thermal resistance. The effect of the shift can be seen in fig. 29. The curves are only shifted with respect to the time. However, the shift results in a change of $T(t = 0)$ and can, therefore, cause significantly higher deviations due to the square-root-fit in the case of strongly shifted transients. The absolute difference for T_0 for a time shift variation of around 1 ms ca be estimated to 3°C and beyond

depending on the shift and the fit range.

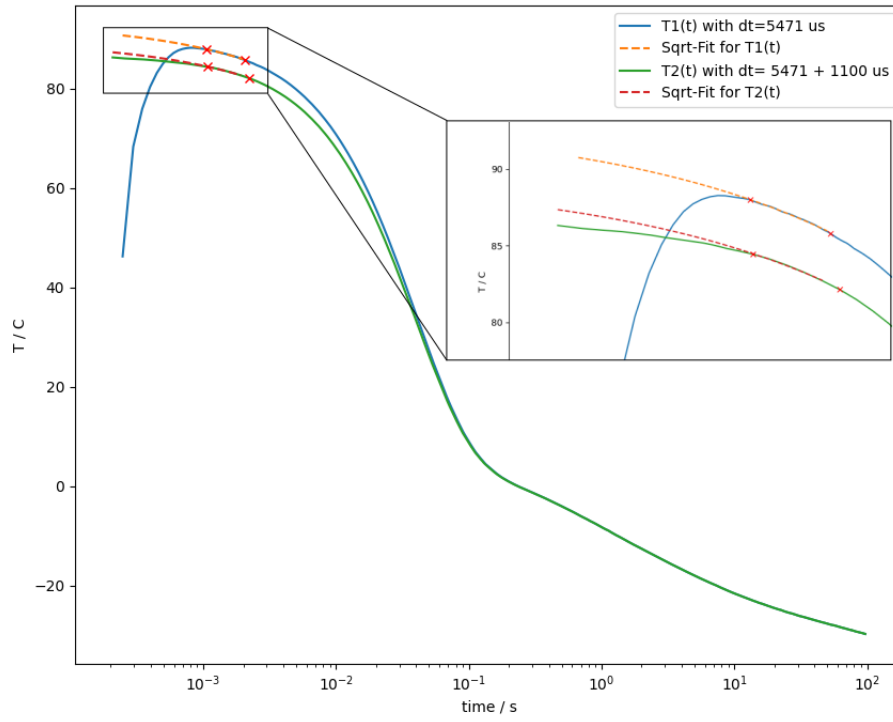


Figure 29: Identical temperature transient with two different time shifts resulting in different initial temperatures after square root fit.

6 RC-network reduction

The actual number of RC elements needed to represent the temperature transient response of a given LED system should be in the same range as the number of layers and layer interfaces. The higher the number of RC elements, the closer the thermal response can be matched with the measured signal. In practice, however, at some point further RC elements do not improve the result anymore. Hence, it is beneficial to use a fewer number of elements, which can directly be associated with physical layers or properties of the system. Every element in the reduced RC-network can represent a real layer or interface of the system. With these elements, further analysis in the scope of failure modelling can be made. By changing only one specific value in the network, the temperature transient behaviour can be rebuilt and compared with actual measurements. Depending on a RC element with different values, which may be related to some failure types, the temperature transient looks different.

6.1 Temperature transient reconstruction from RC-networks

The goal of the network reduction is to reconstruct the measured temperature transient of the given measurement device. Once the temperature transient is known one can calculate the structure function, which yields to the different thermal resistances of the layers. Up to this point, the structure function calculation contains 200 RC elements, which is a compromise of high resolution and numerical computation. However, the structure function can be used to create a new RC-network with a reduced number of RC elements to approximate the original transient.

In fig. 30 the reconstruction process is shown. Beginning with a reduced RC-network, the first task is to transform the Cauer network into the Foster network. Even though a solution for the Cauer network can be calculated, it is much easier to obtain the transient response from the Foster network. It allows you to directly compare measurement values without further manipulation of the measurement data. This is a huge advantage, because the quantitative comparison can be done with a weighted cost function, in which errors can be estimated with respect to a certain time range of interest.

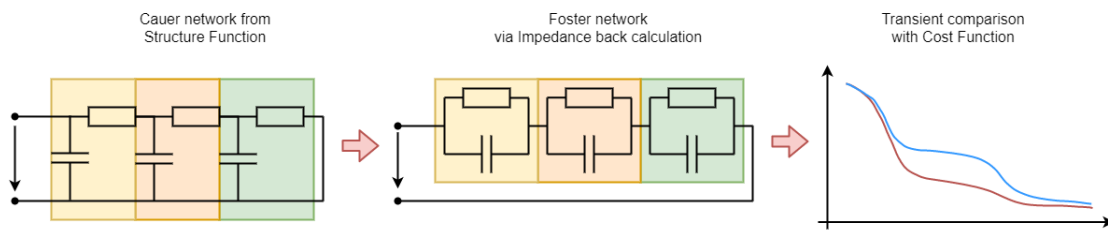


Figure 30: Flow chart for transient reconstruction

6.1.1 Network transformation from Cauer network to Foster network

Recall that in the calculation process of the structure function, the Foster network as first RC network representation (based on the calculation process of the structure function) must be transformed to the Cauer network. The Cauer network represents the physical structure, which allows a layer based interpretation. However obtaining the temperature transient by solving the Cauer network is far more difficult. Finding the solution with an analytical approach can be done by solving the unknown quantities with the Kirchhoff laws. Applying these laws one obtains differential equations whose order corresponds to the number of RC elements: eqs. (11)

and (13) show the solutions for first and second order equations. The solution of the first order equation is represented by an exponential decay.

$$\frac{dU(t)}{dt} - \frac{1}{RC}U(t) = 0 \Leftrightarrow \quad (11)$$

$$U(t) = U_0 e^{-\frac{t}{RC}} \quad (12)$$

For the second order, the relation $U_{C_1} = U_{R_1+R_2}$ is used to calculate the solution for the junction to ambient voltage. The solution contains two exponential functions, where the RC values define their behaviour.

$$R_1 C_1 C_2 \frac{d^2 U_{C_1}}{dt^2} + (C_1 + C_2 + C_1 \frac{R_1}{R_2}) \frac{dU_{C_1}}{dt} + \frac{U_{C_1}}{R_2} = 0 \Leftrightarrow \quad (13)$$

$$\text{Solution with Ansatz: } U_{C_1}(t) = A_1 e^{t\lambda_1} + A_2 e^{t\lambda_2} \quad (14)$$

To avoid differential equations one can use the Laplace transformation and change to the s-space. The back transformation is done with the impedance quantity $Z(s)$. Equations (15) to (21) show the ansatz and recursion formula for $Z(s)$.

$$Z_{Foster}(\omega) = Z_{Cauer}(\omega) \quad (15)$$

$$\sum_{i=1}^n \frac{R_{f,i}}{1 + i\omega C_{f,i}} = \frac{1}{i\omega C_{c,1} + \frac{1}{R_{c,1} + \frac{1}{i\omega C_{c,2} + \frac{1}{R_{c,2} + \dots}}}} \quad (16)$$

$$(17)$$

Since both Cauer and Foster networks have the same impedance, one can back calculate the resistance values R_i and capacitance values C_i for each network. The term for the Cauer network consists of multiple nested fractions which can be rewritten as fraction of two polynomials $P^{(n-1)}(s)$ and $Q^{(n)}(s)$ of order $n - 1$ and n .

$$s = i\omega \quad (18)$$

$$P_0 = 0, Q_0 = 1 \quad (19)$$

$$\frac{P_n}{Q_n} = \frac{R_n Q_{n-1} + P_{n-1}}{s C_n (R_n Q_{n-1} + P_{n-1}) + Q_{n-1}} \quad (20)$$

$$Z_{Cauer}(s) = \frac{P^{(n-1)}(s)}{Q^{(n)}(s)} = \sum_{i=1}^n \frac{A_i}{s - s_i} \sim Z_{Foster}(s) \quad (21)$$

The fraction of polynomials can be reduced further with a partial fraction decomposition to get an equivalent form for the Foster network. The calculation is described further in [37].

The partial fraction decomposition includes the numerical computation of polynomial roots. This works well for polynomials of order below $n = 30$, depending on the algorithm. In this context, this limitation does not pose a problem, since the number of layers should be less than 30. Calculating the Foster network elements, the RC values can reconstruct the temperature response of the system, as discussed in the following section.

6.1.2 Temperature response validation with cost function

Knowing the RC elements of the Foster network the temperature transient can be calculated with the given formula from section 6.1.2.

$$T(t) = \sum_i R_i \cdot e^{\frac{t}{RC}} \quad (22)$$

This formula has a big advantage for the comparison to the original data. The data points can be calculated for each time at which T was acquired in the experiment. Therefore no extrapolation has to be done. The expression can be used to directly formulate a cost function to determine the deviation of the prediction from the measured data. The cost function $E[(T_i, t_i)_{measurement}]$ is defined below, where $T_{measurement}$ is the measurement data, T_{model} is the model basis from the Foster network and $\Omega(t)$ is the weight function. Usually the weight function Ω is defined to ensure a higher accuracy for short time stamps, since these contain most of the information associated with the physical layers.

$$E[(T_i, t_i)_{measurement}] = \sqrt{\frac{1}{n} \sum_{i=1}^n \Omega(t_i) \cdot (T_{measurement,i} - T_{model}(t_{measurement,i}))^2} \quad (23)$$

The design of the weight function is not restricted to any rule, nevertheless it is useful to normalize it. Examples for such functions including the identity function are shown in fig. 31.

6.2 Network reduction with structure function

For a deeper understanding the structure function is reduced in several ways. It is essential to understand how the different RC elements build the network for a physical temperature transient. The reduction of the structure function leads to the consequence that the reduced network transient can be different at some points compared to the original measurement. In order to avoid that, the number of RC elements must be chosen adequate, such that extreme fluctuations are prevented. There is no precise upper bound for an RC network to get a good match of the measurement data with the theoretical solution. There is also no “perfectly” reduced solution because fewer elements typically lead to more inaccurate results for the structure function. The strategy to obtain the “best” temperature transient response according to the structure function is trial and error. To get a better picture, how important each RC element contributes to the temperature transient, the following methods are investigated to find a proper reduction.

- **Cluster average values**, divide structure function into clusters and take average value
- **Index values**, take every n -th RC element in the network
- **Structure function peaks**, take the highest peaks for $\frac{dC_{th}}{dR_{th}}$
- **Structure function plateaus**, take the highest peaks for $\frac{dR_{th}}{dC_{th}}$ (equivalent to midpoint of plateau for $\frac{dC_{th}}{dR_{th}}$)

In figs. 32 to 35 the reduced structure function with reproduced temperature transients for these four different reduction methods are shown. The number of RC elements are chosen to be $n = \{5, 11, 20\}$. Regardless of the method, these figures clearly show that transients based on a higher number of RC elements reproduce the original measurement better. One can use the cost function with specified weights to get a better quantification, how well the transient response is mapped. For comparison, an unweighted cost function and a weighted cost function is used. The design of the weight functions is shown in fig. 31. The weighted function should increase the

focus on the short time spans (ns to ms) of the transient and reduce the significance for time spans above 10 s.

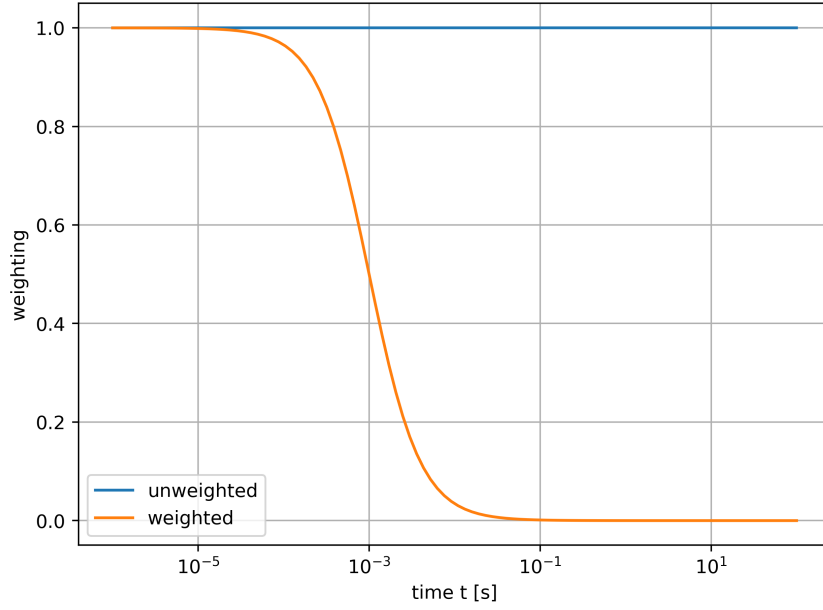


Figure 31: Weight functions for the cost function to calculate the deviation from the original transient measurement. Weight function $\Omega(t) = \frac{1}{1+e^{(\log_{10}(t)-3)/0.3}}$

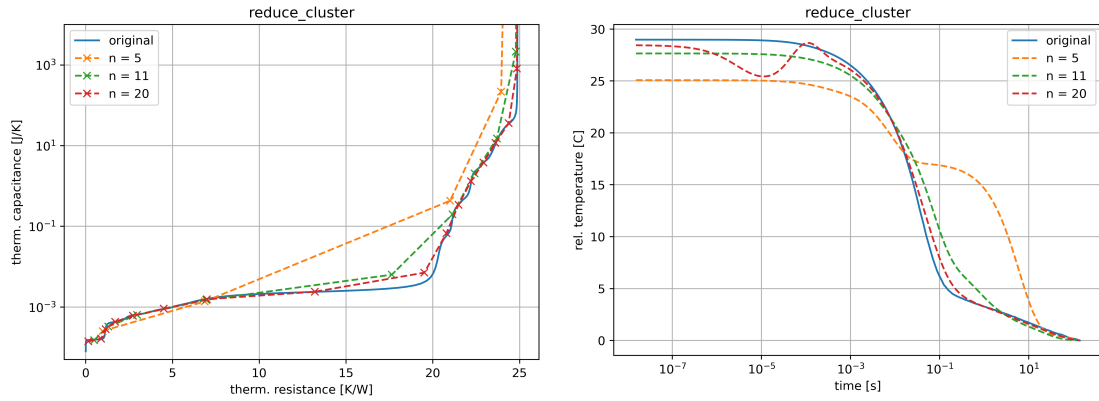


Figure 32: Reduction results for cluster average method. Left graph: original and reduced structure functions. Right graph: temperature transient comparison with original measurement data and reproduced transient. Number of RC elements for reduced networks: $n = 5, 11, 20$.

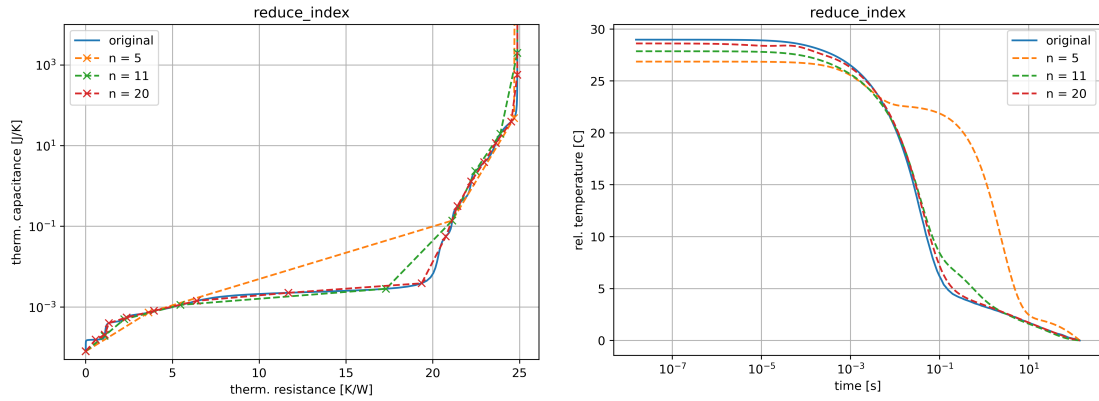


Figure 33: Reduction results for index values method. Left graph: original and reduced structure functions. Right graph: temperature transient comparison with original measurement data and reproduced transient. Number of RC elements for reduced networks: $n = 5, 11, 20$.

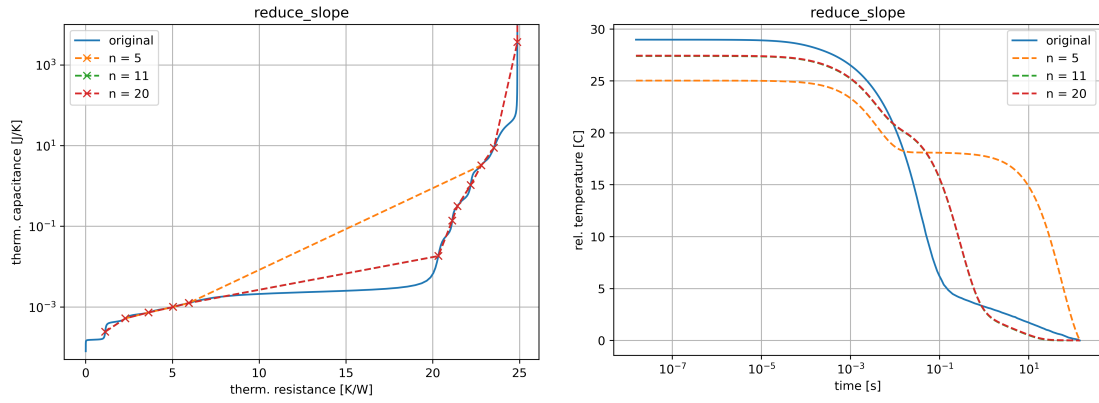


Figure 34: Reduction results for structure functions slopes method. Left graph: original and reduced structure functions. Right graph: temperature transient comparison with original measurement data and reproduced transient. Number of RC elements for reduced networks: $n = 5, 11, 20$.

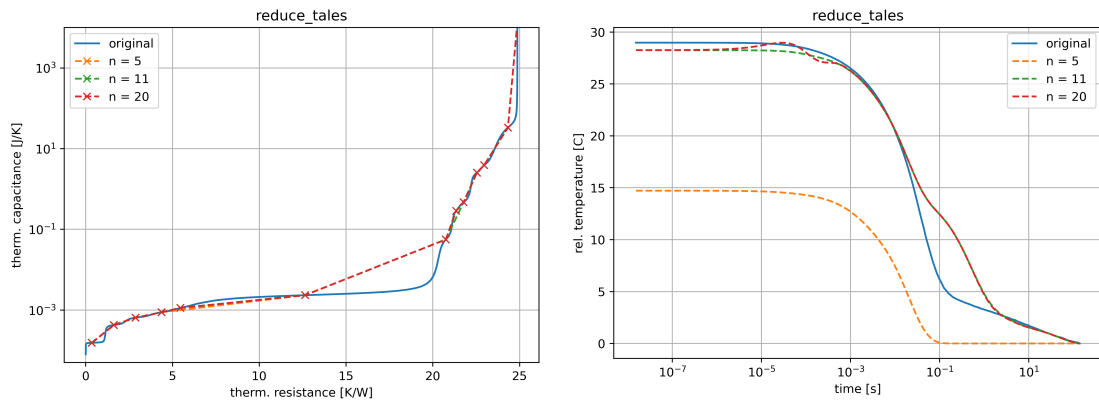


Figure 35: Reduction results for cluster average method. Left graph: original and reduced structure functions. Right graph: temperature transient comparison with original measurement data and reproduced transient. Number of RC elements for reduced networks: $n = 5, 11, 20$.

In fig. 36, the errors between the reduced model and the true measurement values for the weighted and unweighted cost functions are shown. The original RC network was reduced to $n = 3..24$ RC elements, where each reduction method was used. It shows in more detail once again the error of the reduced network transient with the original transient. Table 3 shows the errors vs. the number of elements in the reduced network for each reduction method.

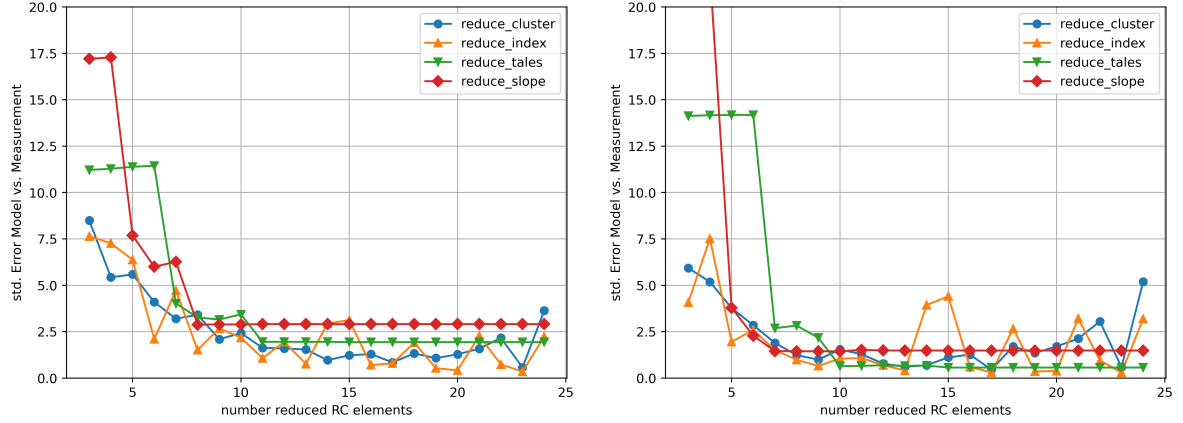


Figure 36: Deviation errors (in °C) between the reduced model and the measurement data for different reduction methods. On the left side the errors are computed unweighted, on the right side the errors are computed with the weight function from fig. 31.

Table 3: Number of RC elements for best reduction (n_{opt}) according to the cost functions (unweighted and weighted)

Reduction method	unweighted		weighted	
	n_{opt}	error / °C	n_{opt}	error / °C
Cluster average	23	0,57	17	0,45
Index values	23	0,35	23	0,29
SF tale	15	1,94	15	0,57
SF slope	8	2,88	10	1,45

Summarizing the results from the reduction analysis, one can state that also few RC elements can represent the measurement system. These reduction methods do not calculate the optimal RC-network for a given number n RC elements, it is just an approximation based on the cost function and the visual comparison of the transient. Even though the index value method is not a layer based split-up, it still matches the temperature transient with lowest error. More complex methods like the structure function slope method or the cluster average method have a higher error value. This larger error implies that a reduced RC-network might look quite different than a full structure function based RC-network.

7 Inline monitoring

In this chapter the implementation of the monitoring process for the thermal resistance of the LED system (DuT) will be described. As claimed, the monitoring of the thermal resistance has to work “inline”, which means the evaluation happens right after the measurement. The LED is stressed non-stop via power cycles (high/low power levels = On / Off) to simulate the life time cycle under service. In the On state the LED system is heating up. When jumping in the low power mode (Off switch), the cooling-down process is recorded as a transient response with the TSEP measurement unit. Using the transient measurement, the thermal resistances can be analysed by determining the structure function. The structure function allows a detailed analysis of the specific layers of the system (LED + mounting). Special layers of interest may be the soldering and interconnection of the PCB to the heat sink (TIM). By combining transient measurements and structure functions, the thermal resistances can be calculated for each cycle, which enables thermal resistance profiling for specified layers in the system over time.

7.1 Monitoring process flow

The monitoring process contains three tasks. The first task is to record the temperature transients as voltage measurements. The second task is to evaluate the structure functions for analysing the thermal resistances. The third part is to analyse and visualize the data so that a detailed insight is possible. The tasks are shown as a sketch in fig. 37. The three tasks do not have to be done by three separate devices, it is just a matter of resources to perform measurement and processing.

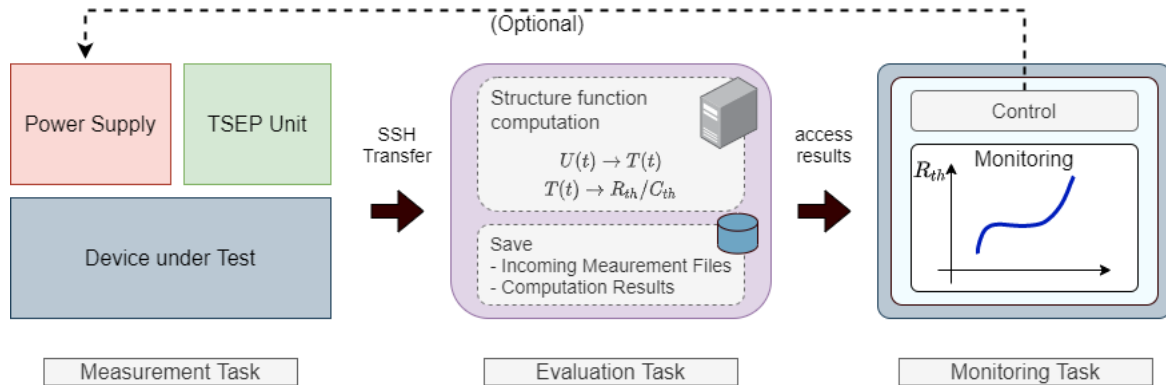


Figure 37: Sketch of the three separate tasks for inline monitoring. Measurement task including device under test, power supply and TSEP unit. Evaluation task for computing the structure function and monitoring task to visualize the thermal resistances.

Measurement task

The measurement setup consists of three devices. The LED is the device under test (DuT), which shall be investigated. It is suitable to put the DuT in a closed environment with fixed external conditions. These external conditions can be temperature, humidity and other factors, which can have impact on the performance and life time of the DuT. A possible setup is shown in fig. 38.

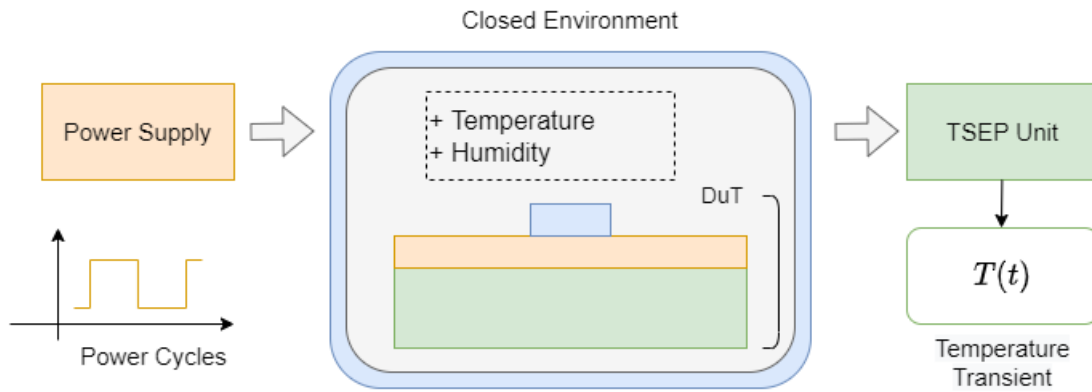


Figure 38: Sketch of the measurement task. Power supply applying the power cycles to the device under test (DuT) which is enclosed with fixed environment parameters. TSEP unit records transient measurements.

The TSEP unit in combination with the power supply performs the measurement task. The power supply addresses power cycles to the DuT, which contain “high power” levels and “low power” levels. The transition from higher to lower power, that is intended to cause a temperature drop in the DuT, is recorded with the TSEP unit. The TSEP unit catches the falling voltage signal and records the voltage transient resulting from the temperature changes. In order to get a highly resolved transient, the power supply itself is required to switch with a fast switching rate. Each cycle enables a continuous monitoring over time and will send related data to a remote server, where all measurement files are stored.

Evaluation task

For each measurement cycle a measurement file (ca. 4 MB) will be transmitted to a remote server with enough storage to save all the files. Since each cycle is recorded and each file containing data finely resolved in time has a rather large size, data management has to be taken into account: All files containing a voltage transient measurement will be evaluated by the server directly when transmitted. The voltage signal is converted to a temperature transient and used to calculate the structure function. The complete calculation is done by a program running on the server using the calculation process from section 5. The results are saved on the server, including the structure function values with the thermal resistances for the monitoring. This interim calculation is done solely due to the extreme data size of the measurement files. The processed results are a fraction in storage capacity and hold much more useful information. Further advantages of relying on server processed data are a much faster analysis and a possibility to visualize the data at any place.

Monitoring

Using the already calculated structure functions for each measurement cycle, the thermal resistance for different layers of the DuT can be monitored. With the structure function, the different layers of the system (DuT + mounting) are visible: Since one can define sections in the structure function that represent physical layers, the R_{th} profile is revealed by plotting these sections over time. First the sections are defined with fixed thermal capacitance values. The procedure is shown in fig. 39. Usually layers can be associated with steps in the structure function. These steps are enclosed with almost vertical lines, where the thermal resistance barely changes. This is the optimal place to set marker points. Marker points are defined as thermal capacitance values (C_{th}), where the thermal resistance (R_{th}) does not change much. The monitoring process

uses these markers to determine the thermal resistances at the start and end point. The thermal resistance difference ΔR_{th} is assigned to the thermal resistance of the layer in the measured system.

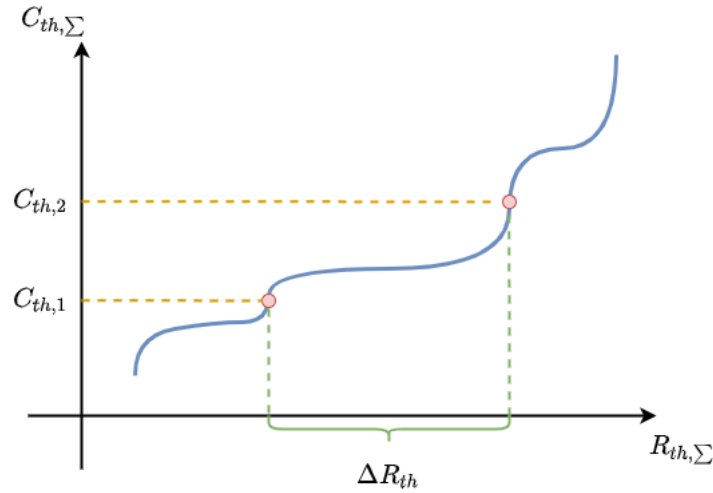


Figure 39: Procedure for setting marker points in the structure function. By choosing two thermal capacitances on the structure functions, a thermal resistance ΔR_{th} can be defined. This selection of the thermal resistances is used for the profile monitoring.

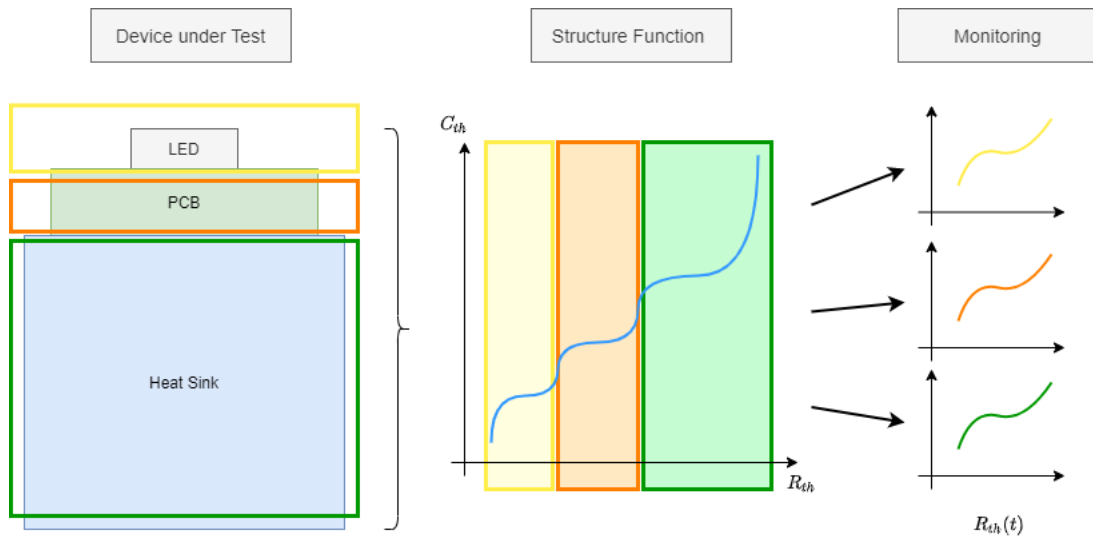


Figure 40: Principle of the marker sections. Each section in the structure function represents a layer in the device under test. These sections are evaluated for each measurement cycle to get a monitoring profile over time.

With the markers it is possible to trace every section in the structure function. The idea is shown in fig. 40. It relates layers of the system to sections in the structure function, which can be monitored with power step transient measurements over time. In principle, one first validates the layers of the system with the steps in the structure function to ensure the right thermal resistance assignment [33]. This is important to conclude certain failure mechanisms from the measurements [23].

7.2 Long term test

The concept of inline monitoring can be implemented via a long term test. The long term test contains power step cycles over a long time compared to the life time of device under test. The LED from section 3 is used to get thermal resistance profiles and analyse the temperature evolution during work load. The main goal is to use the structure function code together with the measurement unit to create an analysis tool, providing the information on thermal resistance profiles.

7.2.1 Experimental setup

Three of two clusters on the PCB are used for the long-term measurement. The circuit diagram is indicated in the left part of fig. 41. The three clusters are connected in series to the power supply. The single cluster is used for the long-term measurements and is permanently measured by the TSEP unit. The two neighbouring clusters are operated to obtain a reference measurement for neighbour heating effects. The effect of the high power density can sometimes lead to a faster malfunction and the test could be terminated prematurely. The setup settings for the long term test are summarized in table 4.

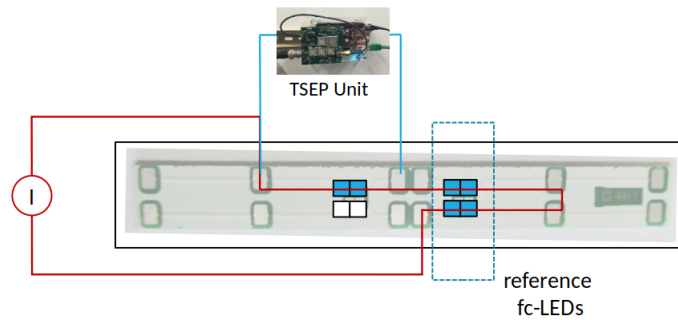


Figure 41: Sketch of the circuit diagram for the device under test. Device under test is connected with to a constant current source and the TSEP unit. The blue squares indicate the powered LEDs. The 4 LED cluster is used for reference measurements comparing neighbour heating effects.

Table 4: Main devices and settings for the long term test.

Device Name	Product Name	Parameters/Notes
Power Supply	Keithley 2260B-80	$t_{heat} = 60\text{ s}$, $t_{cool} = 100\text{ s}$, $I_{heat} = 700\text{ mA}$, $I_{cool} = 10\text{ mA}$, power cycles with constant current mode
Oven	Binder MK-56	Environment temperature $T = 10^\circ\text{C}$, connection port for wiring
TSEP unit	Red Pitaya + TT frontend	Measurement time $t = 200$ (aprox. 96 s), Offset voltage $U = 5.5\text{ V}$, WLAN connection, SHH transmission for files
storage server	Raspberry Pi	LAN connection, evaluation of transient files

The LEDs are measured in an oven with stable temperature conditions. This guarantees, that external influences do not change during testing. The oven is able to heat as well as to cool down

to 10 °C. This allows a wider range of applied power with lower environmental temperature, since the maximal power is dependent on the temperature limitations of the LEDs. Figure 42 shows the structure and wiring in the laboratory. The wiring runs through the side wall of the oven. All LEDs can therefore be measured at any time.

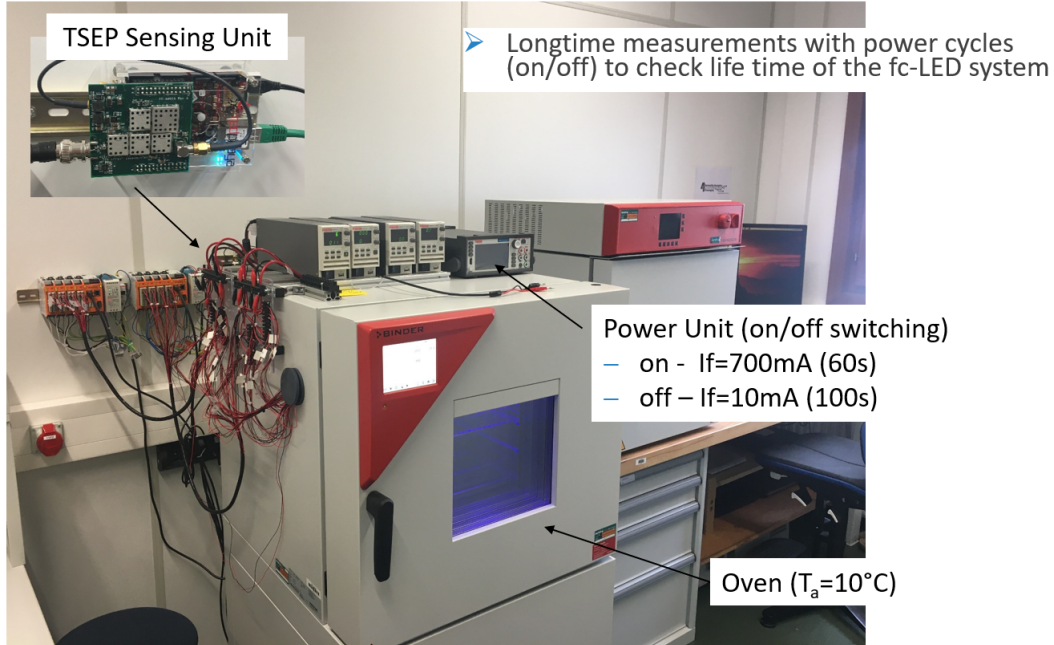


Figure 42: Setup picture, oven with LEDs, TSEP unit for measuring transients and power supply for power cycles.

A Raspberry Pi, which is located in the same network as the TSEP unit, serves as the storage server for processing the measurement data. This allows data to be exchanged via SSH. The data is then stored, evaluated and processed on the Raspberry Pi. This is done with two separate Python programs (development of structure function and visualization).

The marker definitions in the structure functions are shown in table 5. The ranges were set due to significant steps in the structure function shown in fig. 43. It is beneficial to use sharp transitions, because they have less uncertainty when determining the thermal resistances.

Table 5: Marker definitions for the long term test. Marker values define the ranges for the thermal resistance profiles.

Layer Type	start C_{th} [J/K]	end C_{th} [J/K]
Chip I	0	0.00045
Chip II	0.00045	0.001
Soldering	0.001	0.022
PCB I	0.022	0.13
PCB II	0.13	0.7
TIM	0.7	8
Heat Sink	8	2000

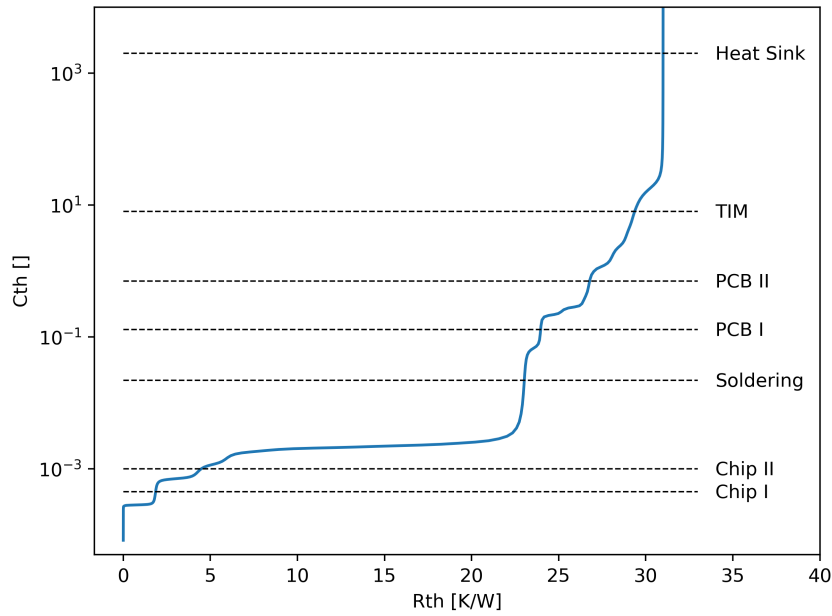


Figure 43: Marker definitions in the structure function for monitoring the DuT. The marker points are set at the front of a step to achieve a small deviation for the thermal resistance.

7.2.2 Results from measurements

In total 21.844 transient measurements were recorded over a run time of 56 days (5.10.-30.11.). During the long-term test there were cuts in the recording. Some problems with the remote server occurred such as memory management or network connection instability due to the long measurement period. Due to these problems, around 2000 measurement were lost. The missing cycles are nonetheless negligible, because the thermal resistances are monitored over time. Although cycles were performed without recording the transients, the evaluation and interpretation of the thermal resistances is possible. Further there are gaps in the profiles, where the power cycle was stopped, because of health check measurements. In this time the LEDs were not stressed but turned off and rested.

For each transient measurement, the thermal resistance was calculated using the code for calculating the structure function. The thermal resistance therefore can be used to describe the state of the LED over time. This is shown in fig. 44. The data points together with its mean value show the evaluation of the thermal R_{th} . It can be seen that the resistance in the sections with continuous recording increases monotonically over time. After some gaps level transitions can be recognized, which show the failures of the other LEDs. On the 6th of November, the first failure of the neighbouring LED occurred, which led to an interruption in the measurements. The remaining two LEDs continued to operate, reducing the overall thermal resistance for the test LED.

The heat produced by the other two LEDs is large enough to slow down the cooling of the entire system. The heat cannot dissipate quickly enough, resulting in a heat build-up. This is also visible in the partial R_{th} evaluations. The thermal resistance of the LED system decreases when total failure of neighbouring LEDs happen, which can also be seen on the 10th of November. The jumps of the R_{th} are only visible in the back layers (PBC and heat sink). The evaluation of the total R_{th} leads to the conclusion that failures can also be detected indirectly without having to monitor the relevant LEDs. A failure is visible as a jump in the total R_{th} , if the heat flow of the neighbouring LEDs affects the LED being monitored.

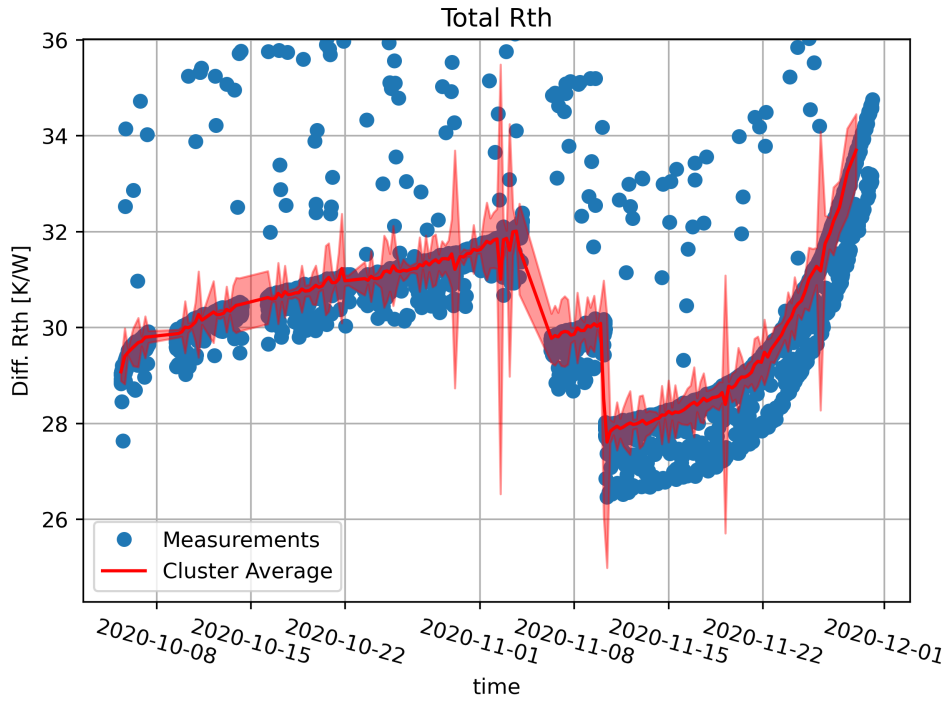


Figure 44: Total thermal resistance of the LED. Data points (blue) describing the calculation result from the transient measurements. Mean value (line) with standard deviation (shaded area) provide the trend. Gaps come from different adjustments or recording problems. Increasing profile over time and jumps after neighbour LEDs fail (6th and 10th Nov.).

In figs. 45 and 46 the partial thermal resistances depending on the markers in the structure function are shown (see table 5). The data points show a broad scattering around the mean value. This comes from the bad resolution of the structure function in the low resistance range. The transition in the structure function is not sharp and wide enough to catch the layers. Therefore no clear statements can be done for this range [38].

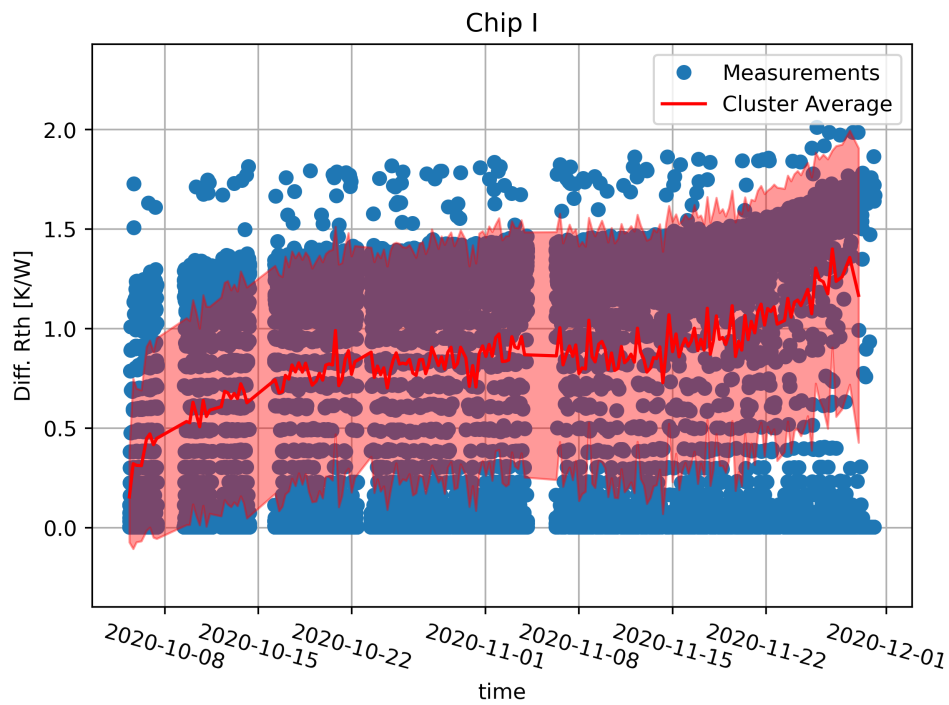


Figure 45: Partial thermal resistance for the marker range “chip I”. Data points describing the calculation results from the transient measurements and mean value with standard deviation as trend. Small change, large standard deviation because of low precision in this resistance range.

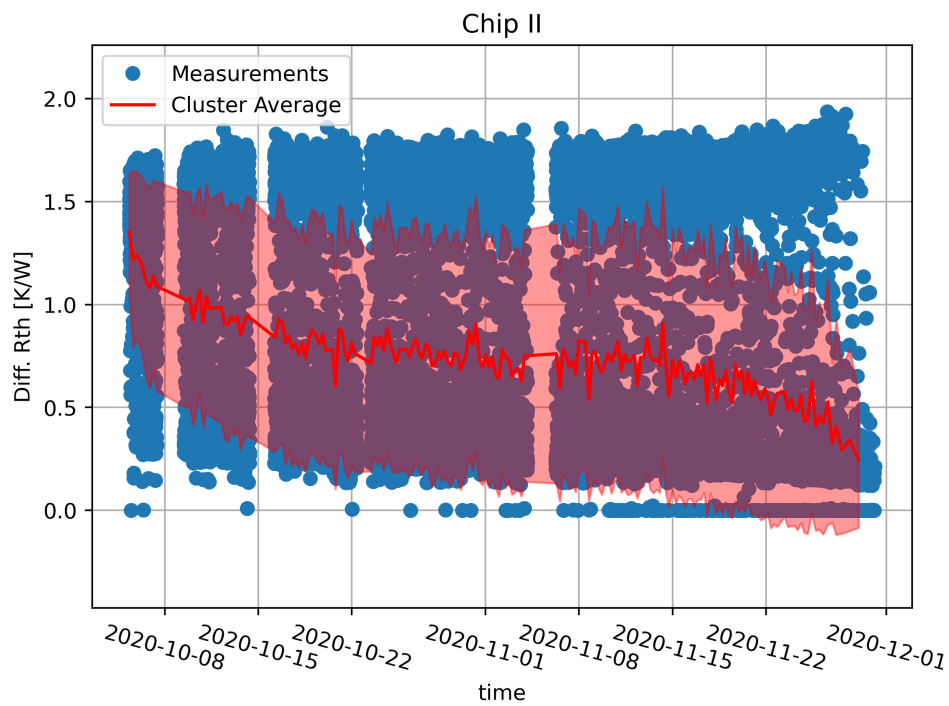


Figure 46: Partial thermal resistance for the marker range “chip II”. Data points describing the calculation results from the transient measurements and mean value with standard deviation as trend. Small change, large standard deviation because of low precision in this resistance range.

The results for soldering layers show the largest changes with over 10 K/W for the thermal resistance (see fig. 47). Many failure types for the LED can be related to this layers. The connection between the LED and the PBC is heavily stressed due to the enormous temperatures and can fail. Reference [1] describes the different possible failure mechanisms, whereas solder joint fatigue relates to failures occurring in this layer. Notably in the last days of operation the thermal resistance increases very fast, which leads to the conclusion that the LED is near at the end of its lifespan. A failure of the test LED was not observed, however the long-term measurement was terminated prematurely.

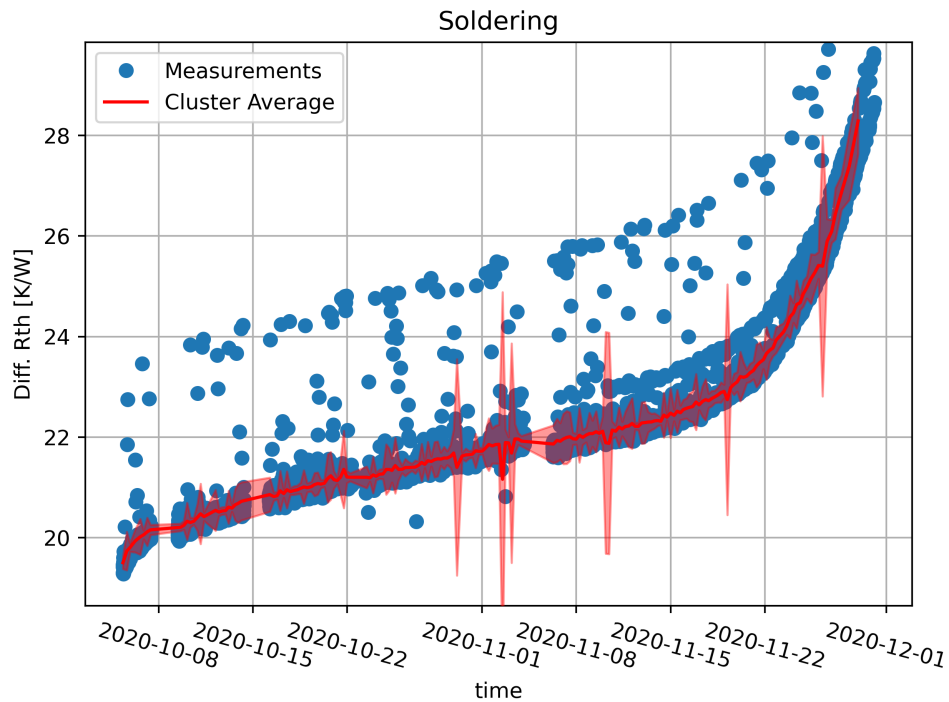


Figure 47: Partial thermal resistance for the marker range “soldering”. Data points describing the calculation results from the transient measurements and mean value with standard deviation as trend. Largest change in thermal resistance, especially for the last days, assuming the LED is near break down.

The thermal resistance profiles for PCB, TIM and heat sink are nearly constant over time, which is shown in figs. 48 to 51. PBC 1 is possibly too close to the soldering section, that is why changes in this profile could also be related to “Soldering”. PCB 2 shows a slight increase before the first LED fails. The increase disappears after the failure, since the heat produced by the remaining LEDs is not sufficient to further attack the material.

The curves for the PCB2, TIM and HS markers show resistance steps after the failure of an LED. As already described, this is due to the fact that less heat can be transported more quickly to the environment. Therefore, failures of neighbouring LEDs as well as the number of failures can be detected without measuring them directly. The drop in partial thermal resistance for failure of a neighbouring LED is around 0.5 K/W per LED.

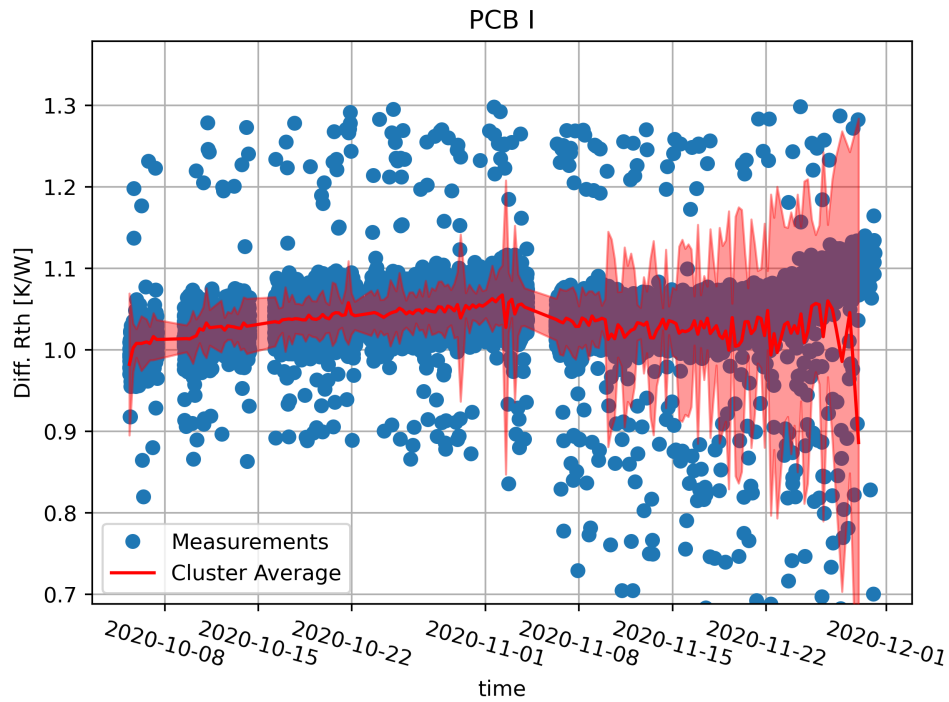


Figure 48: Partial thermal resistance for the marker range “PCB I”. Data points describing the calculation results from the transient measurements and mean value with standard deviation as trend. Marker setting is too close to “Soldering”, therefore thermal resistance is too small to see any dominant profile.

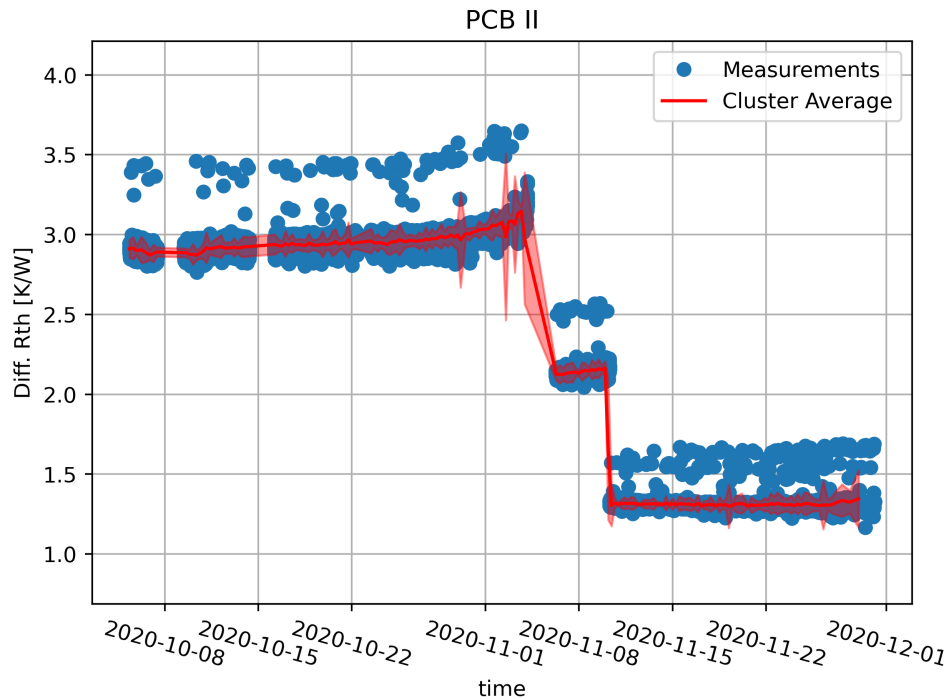


Figure 49: Partial thermal resistance for the marker range “PBC II”. Data points describing the calculation results from the transient measurements and mean value with standard deviation as trend. Almost constant over time, jumps indicating failures of neighbouring LEDs.

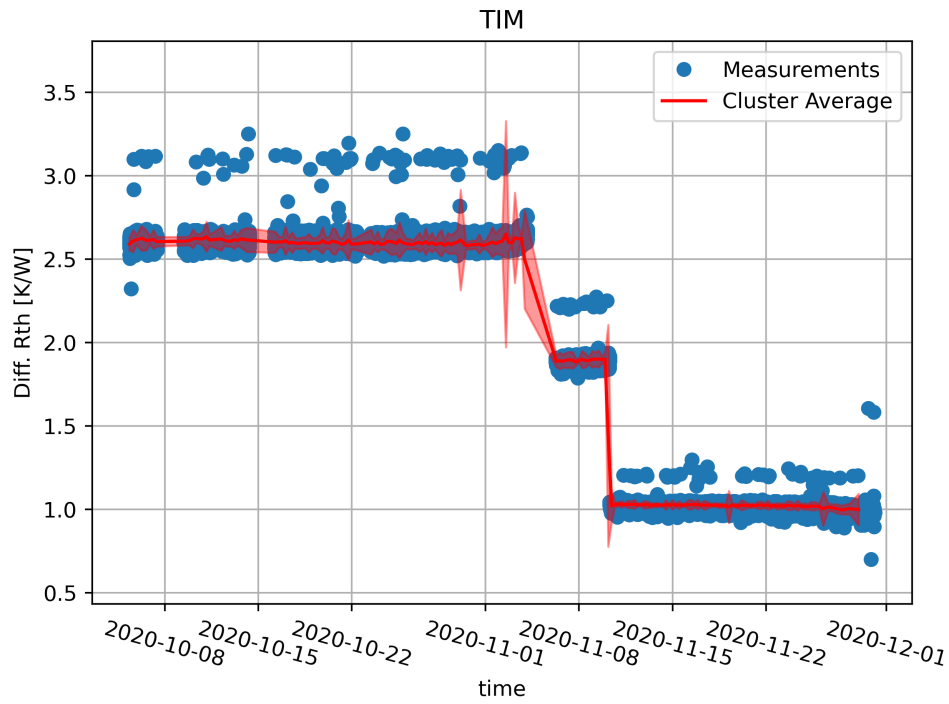


Figure 50: Partial thermal resistance for the marker range “TIM”. Data points describing the calculation results from the transient measurements and mean value with standard deviation as trend. Constant over time, jumps indicating failures of neighbouring LEDs.

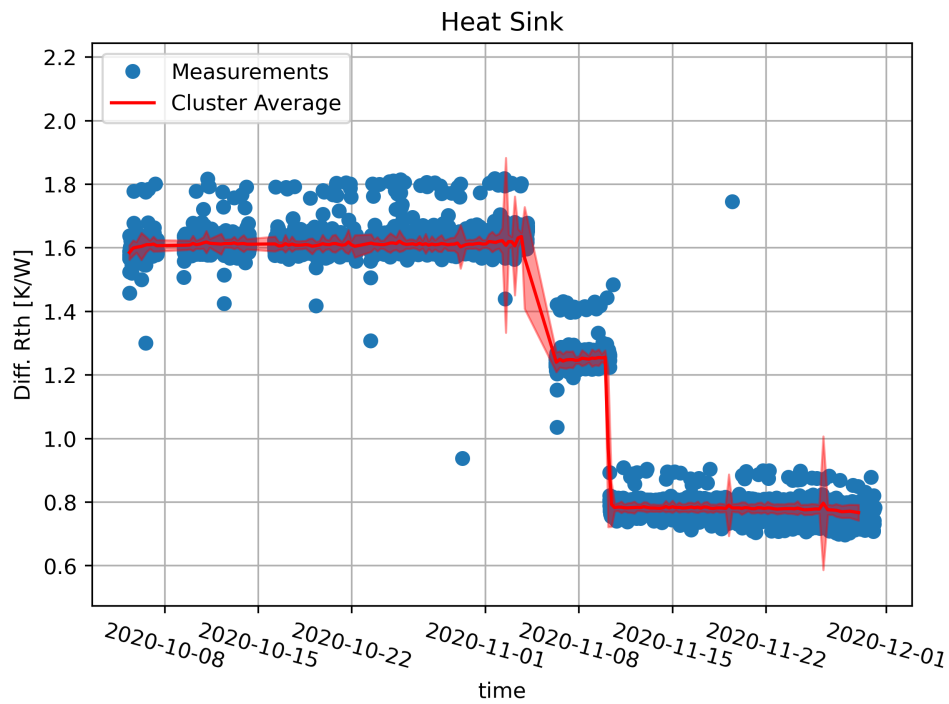


Figure 51: Partial thermal resistance for the marker range “Heat Sink”. Data points describing the calculation results from the transient measurements and mean value with standard deviation as trend. Constant over time, jumps indicating failures of neighbouring LEDs.

8 Summary

The main priority of this work was to set up an in situ monitoring system, which is able to estimate the current lifetime status of an LED. The status of the LED includes information about the age or rather the physical condition of the device. To reveal this information, the setup consists of (i) a measurement part to record the temperature transient response as well as (ii) computation resources with calculation tools that deliver, for example, the structure function. Using the temperature transient resulting from a step response from a power switch to the LED, one is able to investigate the thermal processes of the test device. The TSEP unit was used to record voltage transients of the LED. The temperature values for the investigation of the thermal properties could be obtained via temperature-voltage relations of semiconductors.

A crucial point was to develop the calculation program written in Python to swiftly compute the structure function. The structure function is the basis of the monitoring process for the test device. The program uses the temperature transient to calculate the thermal resistances and capacitances of the system. One goal was to get the calculation time below the measurement time to make it useable on the measurement device or other evaluation devices. It should work “inline”, more specific, it should run within the measurement cycle. Run time tests showed that a full calculation process took less than 1 second, so it is suitable for using it inline. The calculation results of the structure function were checked against the T3ster Master reference instrument. Since measurement part and calculation part have its own variations, cross comparisons with different measurement setups were done. The results matched each other the structure profile and total thermal resistance within an acceptable agreement.

In addition, a long-term test was realized to test the monitoring setup under real conditions. A test LED was connected to the TSEP unit to record transient measurements from power cycles over a longer time. The applied operating power to the LED was set above the standard operating power in order to record the full live cycle of the LED during this long-term test. With the structure function it is possible to mark certain thermal resistance regions, which can be monitored. The regions can be chosen such that they represent physical layers of the device. This enables a separate visualisation for parts of the LED, in which failures can occur. All the visualization was done inline along with every measurement cycle. Therefore, failure analysis was performed live during the long-term test. It showed, that only certain thermal resistance sections changed over time. These sections relate to fatigue failures. Not only failure, but failure types can be detected within this method. After detection, control mechanisms like lower operation power or changes in the setup can be done to prevent the LED from failing.

The structure function calculation of the monitoring setup yields a high number of RC network elements. The number of elements is quite too high to assign physical layers or interfaces to them. In this thesis, it was explored to which extent the number of RC elements can be reduced, while still matching the original temperature transient. For this reduction, methods were designed that reduce the structure function to an adequate number of layers. Via the back transformation algorithm, the original transient can be compared with the reduced transient. The comparison can be done with an individually designed cost function to set preferences for important time sections in the transient. Results showed that a good match with the original transient can be achieved with as few as approximately 30 RC elements in a thermal network. This number is close to model for transients predicted from physical layers.

The long-term testing showed that the monitoring principle is indeed usable. The measurement equipment can be attached to any other LED system, for which temperature transient measurements are possible. Every LED can have its own thermal resistance profile over time, where further investigations can be made such as profile characterisation for different devices. Different devices may also have different failure mechanisms which would be observable in the resistance

profiles from the structure function. Most failure types are related to temperature changes associated with thermal resistance changes. There may be unique patterns, which can relate to certain failure modes. These failure modes can be investigated “inline” with the monitoring setup.

References

- [1] Moon-Hwan Chang et al. "Light emitting diodes reliability review". In: *Microelectronics Reliability* 52.5 (May 2012), pp. 762–782. ISSN: 00262714. DOI: 10.1016/j.microrel.2011.07.063. URL: <https://linkinghub.elsevier.com/retrieve/pii/S0026271411003283> (visited on 05/22/2021).
- [2] Gaudenzio Meneghesso et al. "Reliability of visible GaN LEDs in plastic package". In: *Microelectronics Reliability* 43.9 (2003). Publisher: Elsevier, pp. 1737–1742.
- [3] Carlo De Santi et al. "Reliability of ultraviolet light-emitting diodes". In: *Light-Emitting Diodes*. Springer, 2019, pp. 397–424.
- [4] Felix Wuest et al. "Comparison of temperature sensitive electrical parameter based methods for junction temperature determination during accelerated aging of power electronics". In: *Microelectronics Reliability* 88 (2018). Publisher: Elsevier, pp. 534–539.
- [5] Yvan Avenas, Laurent Dupont, and Zoubir Khatir. "Temperature Measurement of Power Semiconductor Devices by Thermo-Sensitive Electrical Parameters—A Review". In: *IEEE Transactions on Power Electronics* 27.6 (June 2012), pp. 3081–3092. ISSN: 0885-8993, 1941-0107. DOI: 10.1109/TPEL.2011.2178433. (Visited on 07/27/2021).
- [6] Nick Baker et al. "Improved reliability of power modules: A review of online junction temperature measurement methods". In: *IEEE Industrial Electronics Magazine* 8.3 (2014). Publisher: IEEE, pp. 17–27.
- [7] Nick Baker et al. "Junction temperature measurements via thermo-sensitive electrical parameters and their application to condition monitoring and active thermal control of power converters". In: *IECON 2013-39th Annual Conference of the IEEE Industrial Electronics Society*. IEEE, 2013, pp. 942–948.
- [8] J. F. J. M. Caers and X. J. Zhao. "Failure Modes and Failure Analysis". In: *Solid State Lighting Reliability: Components to Systems*. Ed. by W.D. van Driel and X.J. Fan. New York, NY: Springer New York, 2013, pp. 111–184. ISBN: 978-1-4614-3067-4. DOI: 10.1007/978-1-4614-3067-4_4. URL: https://doi.org/10.1007/978-1-4614-3067-4_4.
- [9] M. Rencz et al. "A methodology for the generation of dynamic compact models of packages and heat sinks from thermal transient measurements". In: *IEEE/CPMT/SEMI 28th International Electronics Manufacturing Technology Symposium, 2003. IEMT 2003*. 28th International Electronics Manufacturing Technology Symposium. San Jose, CA, USA: IEEE, 2003, pp. 117–123. ISBN: 978-0-7803-7933-6. DOI: 10.1109/IEMT.2003.1225887. (Visited on 05/31/2022).
- [10] Andras Vass-Varnai et al. "Measurement based compact thermal model creation - accurate approach to neglect inaccurate TIM conductivity data". In: *2011 IEEE 13th Electronics Packaging Technology Conference*. 2011 IEEE 13th Electronics Packaging Technology Conference - (EPTC 2011). Singapore, Singapore: IEEE, Dec. 2011, pp. 67–72. ISBN: 978-1-4577-1982-0 978-1-4577-1983-7 978-1-4577-1981-3. DOI: 10.1109/EPTC.2011.6184388. (Visited on 05/31/2022).
- [11] Vladimir Székely and Tran Van Bien. "Fine structure of heat flow path in semiconductor devices: A measurement and identification method". In: *Solid-State Electronics* 31.9 (1988), pp. 1363–1368. ISSN: 0038-1101. DOI: [https://doi.org/10.1016/0038-1101\(88\)90099-8](https://doi.org/10.1016/0038-1101(88)90099-8). URL: <https://www.sciencedirect.com/science/article/pii/0038110188900998>.

- [12] Nadarajah Narendran et al. “Projecting LED product life based on application”. In: *Fifteenth International Conference on Solid State Lighting and LED-based Illumination Systems*. Ed. by Matthew H. Kane, Nikolaus Dietz, and Ian T. Ferguson. Vol. 9954. Backup Publisher: International Society for Optics and Photonics. SPIE, 2016, pp. 60–67. DOI: 10.1117/12.2240464.
- [13] *Solid State Lighting - 4E Energy Efficient End-use Equipment*. Publication Title: 4E Energy Efficient End-use Equipment; SSL Annex Lifetime Literature Review Report by the LRC. June 2021. URL: <https://www.iea-4e.org/ssl> (visited on 06/18/2021).
- [14] Gordon Elger et al. “Inline thermal transient testing of high power LED modules for solder joint quality control”. In: *2011 IEEE 61st Electronic Components and Technology Conference (ECTC)*. 2011 IEEE 61st Electronic Components and Technology Conference (ECTC). Lake Buena Vista, FL, USA: IEEE, May 2011, pp. 1649–1656. ISBN: 978-1-61284-497-8. DOI: 10.1109/ECTC.2011.5898733. (Visited on 05/31/2022).
- [15] J. Magnien et al. “Reliability and failure analysis of solder joints in flip chip LEDs via thermal impedance characterisation”. In: *Microelectronics Reliability* 76-77 (Sept. 2017), pp. 601–605. ISSN: 00262714. DOI: 10.1016/j.microrel.2017.07.052. URL: <https://linkinghub.elsevier.com/retrieve/pii/S0026271417303360> (visited on 05/31/2021).
- [16] U.S. Department of Energy. “Lifetime and Reliability”. In: (Aug. 2013). Building Technologies Program Solid-state Lighting Technology fact sheet, PNNL-SA-97534.
- [17] IES LM. *IES LM-80-08. Approved method: measuring lumen maintenance of LED light sources*. Illuminating Engineering Society, 2008.
- [18] Jeff Hulett et al. *IES LM-80-20 Approved Method: Measuring Luminous Flux and Color Maintenance of LED Packages, Arrays, and Modules*. Illuminating Engineering Society, 2020. ISBN: 978-0-87995-214-3.
- [19] Illuminating Engineering Society of North America Museum and Art Gallery Lighting Committee. *Technical Memorandum: Projecting Long-term Lumen, Photon, and Radiant Flux Maintenance of Led Light Sources : An American National Standard*. Illuminating Engineering Society, 2019.
- [20] Gordon Elger et al. “Analysis of solder joint reliability of high power LEDs by transient thermal testing and transient finite element simulations”. In: *Microelectronics Journal* 46.12 (Dec. 2015), pp. 1230–1238. ISSN: 00262692. DOI: 10.1016/j.mejo.2015.08.007. URL: <https://linkinghub.elsevier.com/retrieve/pii/S0026269215001962> (visited on 05/31/2022).
- [21] Mesago PCIM GmbH Stuttgart, ed. *PCIM Europe 2014: International Exhibition and Conference for Power Electronics, Intelligent Motion, Renewable Energy and Energy Management Nuremberg, 20 – 22 May 2014, Proceedings*. Investigation of Temperature Sensitive Electrical Parameters for Power Semiconductors (IGBT) in Real-Time Applications. Berlin: VDE Verl, 2014. ISBN: 978-3-8007-3603-4.
- [22] *Thermal Management for LED Applications*. In collab. with Clemens J.M. Lasance and András Poppe. New York, NY: Springer New York, 2014. DOI: 10.1007/978-1-4614-5091-7. URL: <http://link.springer.com/10.1007/978-1-4614-5091-7> (visited on 05/31/2022).
- [23] Lisa Mitterhuber et al. “Thermal transient measurement and modelling of a power cycled flip-chip LED module”. In: *Microelectronics Reliability* 81 (Feb. 2018), pp. 373–380. ISSN: 00262714. (Visited on 05/31/2022).

- [24] Lisa Mitterhuber et al. “Investigation of the temperature-dependent heat path of an LED module by thermal simulation and design of experiments”. In: *2016 22nd International Workshop on Thermal Investigations of ICs and Systems (THERMINIC)*. 2016 22nd International Workshop on Thermal Investigations of ICs and Systems (THERMINIC). Budapest, Hungary: IEEE, Sept. 2016, pp. 194–200. ISBN: 978-1-5090-5450-3 978-1-5090-5451-0. (Visited on 05/31/2022).
- [25] Heinz Pape et al. “Development of a standard for transient measurement of junction-to-case thermal resistance”. In: *2011 12th Intl. Conf. on Thermal, Mechanical & Multi-Physics Simulation and Experiments in Microelectronics and Microsystems*. Multi-Physics Simulation and Experiments in Microelectronics and Microsystems (EuroSimE). Linz, Austria: IEEE, Apr. 2011, pp. 1/8–8/8. ISBN: 978-1-4577-0107-8. DOI: 10.1109/ESIME.2011.5765862. (Visited on 05/31/2022).
- [26] A. Vass-Varnai et al. “Comparison of JEDEC dynamic and static test methods for the thermal characterization of power LEDs”. In: *2012 IEEE 14th Electronics Packaging Technology Conference (EPTC)*. 2012 IEEE 14th Electronics Packaging Technology Conference - (EPTC 2012). Singapore: IEEE, Dec. 2012, pp. 594–597. ISBN: 978-1-4673-4552-1 978-1-4673-4553-8 978-1-4673-4551-4. DOI: 10.1109/EPTC.2012.6507151. (Visited on 05/31/2022).
- [27] Epistar. Epistar ES-FADBPE38D InGaN Blue LED Chip. May 2021. URL: <https://www.epistar.com/EpistarEn/index> (visited on 05/10/2021).
- [28] *Industrie PC auf Raspberry Pi Basis Überblick Revolution Pi*. Publication Title: Revolution Pi. Dec. 2021. URL: <https://revolutionpi.de/revolution-pi-serie> (visited on 12/02/2021).
- [29] Julien Magnien, Lisa Mitterhuber, and Elke Kraker. “Temperature Sensitive Electrical Parameter Sensing Unit for Early Failure Detection”. In: *2019 25th International Workshop on Thermal Investigations of ICs and Systems (THERMINIC)*. 2019 25th International Workshop on Thermal Investigations of ICs and Systems (THERMINIC). Lecco, Italy: IEEE, Sept. 2019, pp. 1–5. ISBN: 978-1-72812-078-2. (Visited on 05/31/2022).
- [30] *Welcome to the Red Pitaya documentation. Red Pitaya 0.97 documentation*. Mar. 2021. URL: <https://redpitaya.readthedocs.io/en/latest> (visited on 03/05/2021).
- [31] Marcelo Luda. *The Red Pitaya Board*. Dec. 2020. URL: https://marceluda.github.io/rp_lock-in_pid/TheApp/RedPitaya_board (visited on 12/02/2020).
- [32] Lisa Mitterhuber. “Evaluation of the thermal behavior of LEDs”. In: (2015), p. 99.
- [33] Lisa Mitterhuber et al. “Validation methodology to analyze the temperature-dependent heat path of a 4-chip LED module using a finite volume simulation”. In: *Microelectronics Reliability* 79 (Dec. 2017), pp. 462–472. ISSN: 00262714. (Visited on 05/31/2021).
- [34] J. Magnien et al. “Parameter driven monitoring for a flip-chip LED module under power cycling condition”. In: *Microelectronics Reliability* 82 (Mar. 2018), pp. 84–89. ISSN: 00262714. DOI: 10.1016/j.microrel.2018.01.005. URL: <https://linkinghub.elsevier.com/retrieve/pii/S0026271418300052> (visited on 05/31/2021).
- [35] JEDEC Standard. “JESD51-1 Integrated Circuits Thermal Measurement Method - Electrical Test Method (Single Semiconductor Device)”. In: *JEDEC Standards* (December 1995), p. 29.
- [36] Transient Dual and Interface Test. “for the Measurement of the Thermal Resistance Junction-to-Case of Semiconductor Devices with Heat Flow Through a Single Path”. In: (November 2010).

- [37] Y.C. Gerstenmaier, W. Kiffe, and G. Wachutka. “Combination of thermal subsystems modeled by rapid circuit transformation”. In: *2007 13th International Workshop on Thermal Investigation of ICs and Systems (THERMINIC)*. 2007 13th International Workshop on Thermal Investigation of ICs and Systems (THERMINIC). Budapest, Hungary: IEEE, 2007, pp. 115–120. ISBN: 978-2-35500-002-7. (Visited on 03/03/2022).
- [38] Dirk Schweitzer et al. “Transient dual interface measurement — A new JEDEC standard for the measurement of the junction-to-case thermal resistance”. In: *2011 27th Annual IEEE Semiconductor Thermal Measurement and Management Symposium*. 2011, pp. 222–229. DOI: 10.1109/STHERM.2011.5767204.

List of Figures

1	Failure rate (dotted lines) and percentage remaining products (solid lines) for two hypothetical products with different life time estimations at 50% failures. [16] . . .	8
2	Lifetime estimation depending on the lumen maintenance, estimation can be done by observing or extrapolating L70/L50 value. [1]	9
3	Transient as step response (process signal) due to instant change of control signal.	10
4	Pictures of LED modules with 8 flip chips EPISTAR mounted on a PCB. Four LED chip cluster (blue frame) with a detail view (yellow frame) of a single chip. Red frame shows an cross section from the chip, the two solder interconnection and the copper core based PCB with an via structure on the back side.	12
5	Setup of LEDs mounted on a PCB which is fixed with wingnuts and springs to ensure equal contact pressure.	13
6	Diode characteristics for a single cluster at different ambient temperatures T_a , at constant current the forward voltage gets lower as the ambient temperature rises.	14
7	Monitoring of the voltage level at a constant measurement current. The plateaus represent the different temperature stages (temperatures 40 °C to 100 °C in 20 °C steps).	14
8	Measurement results, average voltage level at given oven temperature for different measurement currents (blue: 10 mA, orange: 100 mA and green: 300 mA). Black lines represent best fit though measurement data.	15
9	Statistical analysis of K values from the linear fits of the single cluster voltage temperature measurements	16
10	Derating curve of the EPISTAR LED showing the operation area, limited by maximal current and maximal temperature.	17
11	Measurement unit consisting of Red Pitaya and TT-frontent, the incoming signal is connected to the TT-frontent (green top board) which shifts the signal for a given offset voltage, the output is connected to the Red Pitaya (red bottom board) which performs the measurement.	19
12	Working principle of measurement device, power supply does power step and switches to lower current level resulting in thermal transient which is recorded by measurement device.	20
13	Example of two repeated measurements on the same LED with the same setup, the first measurement (blue) shows a significant time shift compared to the second measurement (orange).	21
14	Time shift visualized, the time where the power supply switches is plotted in a histogram, the times are equally distributed since the start is random, maximal time shift 7 ms.	21
15	Comparison between a correct and incorrect measurement with the TSEP measurement device. Left a valid measurement which shows the voltage level as the LED cools down, right the same process but with invalid characteristics namely the straight line and the sharp turn.	22
16	Fit point range (red crosses) for square root fit of $T(t = 0)$ to remove the electrical noise from the power supply. (Note that the absolute temperature values does not match with real values since the offset is not chosen properly.)	26

17	Computation process of the structure function.	26
18	Foster network (above) and Cauer network (below) as byproducts of the calculation process [36]. R_{th} and C_{th} describing the thermal resistances and capacitances in the network.	27
19	Structure function from the Cauer network representation.	28
20	Workflow for comparing two separate structure function evaluation systems. The systems contain its own measurement operation and calculation operation. Left Red Pitaya as a compact system, right comparison device respectively the T3ster Master	29
21	Histogram of thermal resistances obtained for different T3ster measurements, above absolute difference, below relative difference. The mean deviation ΔR_{th} is found at -0.05 K/W.	30
22	Structure functions calculated by the Red Pitaya and the T3ster Master from prerecorded measurement data from the T3ster. Top figure shows the cumulated structure function, bottom figure shows the differential structure function. . . .	31
23	Histogram thermal resistances for different Red Pitaya measurements, above absolute difference, below relative difference. The mean deviation ΔR_{th} is found at -0.22 K/W.	32
24	Structure function evaluation for TSEP measurement, main peaks match with reference calculation, deviations are present for small values.	33
25	Separate temperature measurements with T3ster and TSEP. TSEP curve shifted by an temperature offset of 8 K for visualisation. The calculation process uses temperature differences, therefore the y-axis does not show the absolute values, all temperature values have a constant offset. Red crosses with green dotted line representing the fit for T_0	34
26	Structure function evaluation for TSEP measurement and T3ster measurement separately. Small deviations for some peaks, total thermal resistance match with 0.5 K/W.	35
27	Results from profiling the code with one full calculation. Total time 1.26 s.	36
28	Variation of input parameters. From top: dissipated power ΔP , time shift Δt and temperature-voltage relation factor K	37
29	Identical temperature transient with two different time shifts resulting in different initial temperatures after square root fit.	38
30	Flow chart for transient reconstruction	39
31	Weight functions for the cost function to calculate the deviation from the original transient measurement. Weight function $\Omega(t) = \frac{1}{1+e^{(\log_{10}(t)-3)/0.3}}$	42
32	Reduction results for cluster average method. Left graph: original and reduced structure functions. Right graph: temperature transient comparison with original measurement data and reproduced transient. Number of RC elements for reduced networks: $n = 5, 11, 20$	42
33	Reduction results for index values method. Left graph: original and reduced structure functions. Right graph: temperature transient comparison with original measurement data and reproduced transient. Number of RC elements for reduced networks: $n = 5, 11, 20$	43

34	Reduction results for structure functions slopes method. Left graph: original and reduced structure functions. Right graph: temperature transient comparison with original measurement data and reproduced transient. Number of RC elements for reduced networks: $n = 5, 11, 20$	43
35	Reduction results for cluster average method. Left graph: original and reduced structure functions. Right graph: temperature transient comparison with original measurement data and reproduced transient. Number of RC elements for reduced networks: $n = 5, 11, 20$	43
36	Deviation errors (in °C) between the reduced model and the measurement data for different reduction methods. On the left side the errors are computed unweighted, on the right side the errors are computed with the weight function from fig. 31. .	44
37	Sketch of the three separate tasks for inline monitoring. Measurement task including device under test, power supply and TSEP unit. Evaluation task for computing the structure function and monitoring task to visualize the thermal resistances.	45
38	Sketch of the measurement task. Power supply applying the power cycles to the device under test (DuT) which is enclosed with fixed environment parameters. TSEP unit records transient measurements.	46
39	Procedure for setting marker points in the structure function. By choosing two thermal capacitances on the structure functions, a thermal resistance ΔR_{th} can be defined. This selection of the thermal resistances is used for the profile monitoring.	47
40	Principle of the marker sections. Each section in the structure function represents a layer in the device under test. These sections are evaluated for each measurement cycle to get a monitoring profile over time.	47
41	Sketch of the circuit diagram for the device under test. Device under test is connected with to a constant current source and the TSEP unit. The blue squares indicate the powered LEDs. The 4 LED cluster is used for reference measurements comparing neighbour heating effects.	48
42	Setup picture, oven with LEDs, TSEP unit for measuring transients and power supply for power cycles.	49
43	Marker definitions in the structure function for monitoring the DuT. The marker points are set at the front of a step to achieve a small deviation for the thermal resistance.	50
44	Total thermal resistance of the LED. Data points (blue) describing the calculation result from the transient measurements. Mean value (line) with standard deviation (shaded area) provide the trend. Gaps come from different adjustments or recording problems. Increasing profile over time and jumps after neighbour LEDs fail (6th and 10th Nov.).	51
45	Partial thermal resistance for the marker range “chip I”. Data points describing the calculation results from the transient measurements and mean value with standard deviation as trend. Small change, large standard deviation because of low precision in this resistance range.	52
46	Partial thermal resistance for the marker range “chip II”. Data points describing the calculation results from the transient measurements and mean value with standard deviation as trend. Small change, large standard deviation because of low precision in this resistance range.	52

47	Partial thermal resistance for the marker range “soldering”. Data points describing the calculation results from the transient measurements and mean value with standard deviation as trend. Largest change in thermal resistance, especially for the last days, assuming the LED is near break down.	53
48	Partial thermal resistance for the marker range “PCB I”. Data points describing the calculation results from the transient measurements and mean value with standard deviation as trend. Marker setting is too close to “Soldering”, therefore thermal resistance is too small to see any dominant profile.	54
49	Partial thermal resistance for the marker range “PBC II”. Data points describing the calculation results from the transient measurements and mean value with standard deviation as trend. Almost constant over time, jumps indicating failures of neighbouring LEDs.	54
50	Partial thermal resistance for the marker range “TIM”. Data points describing the calculation results from the transient measurements and mean value with standard deviation as trend. Constant over time, jumps indicating failures of neighbouring LEDs.	55
51	Partial thermal resistance for the marker range “Heat Sink”. Data points describing the calculation results from the transient measurements and mean value with standard deviation as trend. Constant over time, jumps indicating failures of neighbouring LEDs.	55

List of Tables

1	Equivalence of electrical and thermal quantities	10
2	Parameters for LED Chip EPISTAR Es-FADBPE38D [27], (T_a ambient temperature)	12
3	Number of RC elements for best reduction (n_{opt}) according to the cost functions (unweighted and weighted)	44
4	Main devices and settings for the long term test.	48
5	Marker definitions for the long term test. Marker values define the ranges for the thermal resistance profiles.	49

Listings

1	Example command for starting a measurement at Red Pitaya	20
2	File structure of a transient measurement with the Red Pitaya	25